Robust Transceiver Design for SWIPT DF MIMO Relay Systems With Time-Switching Protocol

Justin Bing Lee, *Member, IEEE*, Yue Rong, *Senior Member, IEEE*, Lenin Gopal, *Member, IEEE*, and Choo W. R. Chiong, *Member, IEEE*

***Abstract*—In this article, we investigate a dual-hop simultaneous wireless information and power transfer decode-and-forward multiple-input and multiple-output relay communication system, in which the relay node harvests energy based on the radio frequency (RF) signal transmitted from the source node through the time-switching (TS) protocol to decode and forward the re-encoded information to the destination node. With the consideration of the channel estimation error, the joint optimization of the TS factor and source and relay precoding matrices is proposed with robustness against the channel state information mismatch to maximize the mutual information (MI) between the source and destination nodes. We derive the optimal structure of the source and relay precoding matrices to simplify the transceiver optimization problem under fixed and flexible power constraints. Numerical examples demonstrate that the proposed algorithms with robustness provide better MI performance compared to the nonrobust algorithm.**

***Index Terms*—Decode-and-forward (DF), energy harvesting (EH), imperfect channel state information (CSI), multiple-input and multiple-output (MIMO) relay, robustness, simultaneous wireless information and power transfer (SWIPT), time switching (TS).**

I. Introduction

RECENTLY, the application of the simultaneous wireless information and power transfer (SWIPT) technology in energy-limited wireless systems has attracted much attention from researchers around the world. This is due to the capability of the SWIPT technology to prolong the lifetime of a wireless system by harvesting energy from radio frequency (RF) signals while receiving information data from the transmitter. In practice, there are two types of SWIPT receivers, which are known as time-switching (TS) and power-splitting (PS) SWIPT receivers [1].

In a scenario where the source and destination nodes are located over a long distance, it is necessary to deploy relay nodes for the wireless system. By utilizing the relay technology, the network coverage of wireless communication is extended [2]. There are mainly two types of relaying schemes commonly used in practice, which are known as the amplify-and-forward (AF) scheme and the decode-and-forward (DF) scheme. The AF relaying scheme amplifies the received signal and forwards it to the next node, while the DF relaying scheme decodes the received information and then encodes it before forwarding the information signal to the next node. In [3], the TS and PS protocols for the SWIPT receiver were adopted to wireless relay systems by introducing TS-based and PS-based relaying protocols to perform energy harvesting (EH) and information decoding (ID) from the received signal at the relay node. The SWIPT relay node processes and forwards the received signals to the destination node by utilizing the energy harvested.

The multiple-input and multiple-output (MIMO) technique, by installing multiple antennas at nodes, is capable of improving the spectral efficiency of a relay system [4]. MIMO relay communication systems with application of SWIPT relay node have been investigated in [5]–[8], [10], and [11]. In [5], Xiong *et al.* investigated the dual-hop SWIPT AF MIMO orthogonal frequency-division multiplexing relay system and developed the TS and PS protocols for the relay system. In [6], SWIPT AF massive MIMO relay networks with PS-based and TS-based relaying schemes were investigated. The authors derived the asymptotic harvested energy and sum rate expression for a relay with an infinite number of antennas. In [7], the joint optimization problem in maximizing the mutual information (MI) between the source and destination nodes for SWIPT AF MIMO relay communication systems with the TS-based relaying scheme was investigated. The joint optimization problem was solved by using the primal-decomposition-based algorithm and the upper-bound-based algorithm. In [8], Li *et al.* investigated a two-hop SWIPT AF MIMO relay communication system with the PS-based relaying scheme. The source and relay precoding matrices with the PS factor matrices were jointly optimized by the sequential quadratic programming approach, the semidefinite programming approach, and the primal-dual search approach to achieve the maximal system MI. In [9], relay-assisted SWIPT was proposed for dual-hop MIMO relay systems, where a half-duplex multiantenna relay node adopts the DF relaying strategy for information forwarding. The PS-based relying protocol is employed to harvest energy from the source transmission. In [10], Li *et al.* extended the work in [7] and [8] to a dual-hop SWIPT DF MIMO relay communication system. In [11], an innovative SWIPT relaying scheme known as the hybridized power-time splitting-based relaying (HPTSR) protocol was presented, where the TS-based and the PS-based relaying

Manuscript received 18 May 2021; revised 2 October 2021; accepted 14 November 2021. Date of publication 8 December 2021; date of current version 9 December 2022. *(Corresponding author: Yue Rong.)*

Justin Bing Lee is with the Custom Logic Engineering Programmable Solution Group, Intel Corporation, Bayan Lepas 11900 Penang, Malaysia (e-mail: justin.bing.lee@intel.com).

Yue Rong is with the School of Electrical Engineering, Computing and Mathematical Sciences, Curtin University, Bentley, WA 6102, Australia (e-mail: y.rong@curtin.edu.au).

Lenin Gopal and Choo W. R. Chiong are with the Department of Electrical and Computer Engineering, Curtin University, Miri 98009 Sarawak, Malaysia (e-mail: lenin@curtin.edu.my; raymond.ccw@curtin.edu.my).

Digital Object Identifier 10.1109/JSYST.2021.3128678

protocols were combined in the HPTSR scheme. The joint optimization for the TS factor, the source and relay precoding matrices, and the PS ratio matrix was tackled to maximize the system MI.

For SWIPT relay systems, it is assumed in [5]–[8], [10], and [11] that the exact channel state information (CSI) is available. However, the exact CSI is unobtainable in practice due to the mismatch between the exact CSI and the estimated CSI. The channel mismatch between the exact and estimated CSI deteriorates the performance of the proposed relay systems [12], [13]. Studies regarding the imperfect CSI in SWIPT MIMO relay systems have been carried out in [14]–[18]. In [14], a dual-hop SWIPT MIMO AF relay communication system was investigated for the ideal EH scheme, the PS-based relaying scheme, and the TS-based relaying scheme. However, the authors only considered the imperfect CSI when optimizing the SWIPT MIMO AF relay communication system with the TS-based relaying scheme. In [15], Benkhelifa *et al.* extended the work in [14] to a DF relay communication system. Similarly, the impact of the imperfect CSI was considered for the TS-based relaying scheme. It is noted that the imperfect CSI considered in [14] and [15] is a special case, where the authors assumed scaled identity matrices as the row and column covariance matrices of the CSI mismatch matrices, and the CSI mismatch is treated as noise. However, in many practical applications, there is channel correlation [19], [20]; hence, the correlation matrix is not an identity matrix. Thus, the assumption made in [14] and [15] is not valid.

In [16], a dual-hop multirelay SWIPT wireless communication system with the TS-based relaying protocol was investigated with the consideration of CSI mismatch, where the communication between the multiantenna source node and destination node is carried out with the help of multiple single-antenna relay nodes. In [17], Shaik *et al.* investigated a SWIPT MIMO AF relay communication system with imperfect CSI. The TS-based relaying protocol was used to perform EH and ID at the relay node, and the transmit antenna selection strategy was used to reduce the system complexity. In other words, the system nodes that transmit information, e.g., the source node and the relay node, are treated as single-antenna system nodes for signal transmission. In [18], an energy-efficient design for a two-way MIMO relay network with the PS-based relaying protocol was investigated with the consideration of the CSI mismatch. It is observed that the CSI mismatch considered in [18] is modeled based on the Euclidean-norm-bounded model. The robust transceiver design based on the Euclidean-norm-bounded CSI mismatch is commonly known as the worst-case based design, which is formulated as a min–max optimization problem, where the "max" is for the worst-case CSI mismatch. The worst-case-based robust design tends to be pessimistic compared with the probability-based robust design.

Different to [14]–[16] and [18], the well-known Gaussian–Kronecker model is adopted in this article to model the CSI mismatch. The Gaussian–Kronecker model is used because in many practical scenarios, there is correlation between the elements of the CSI mismatch matrix. Different to [16], the system nodes considered in this article are all equipped with multiple antennas. Moreover, in contrast to [17], in this article, all system antennas considered are used.

We propose a transceiver design for a dual-hop MIMO relay communication system with a SWIPT relay using the DF relaying protocol. The transceiver is designed with the consideration of imperfect CSI. We would like to mention that the implementation of the robust SWIPT DF MIMO relay system can be done in a similar way to those nonrobust designs. The focus of this article is on the system optimization. To the best of our knowledge, there is no existing work carried out in SWIPT DF MIMO relay systems with consideration of imperfect CSI modeled based on the Gaussian–Kronecker model. We show through numerical simulations that the proposed scheme improves the robustness of SWIPT DF MIMO relay systems against the channel estimation error.

The contributions/challenges of this article are summarized as follows.

1) The impact of the channel estimation error modeled by the Gaussian–Kronecker model on the performance of a dual-hop SWIPT DF MIMO relay system is examined in this article. To the best of our knowledge, there is no existing work carried out in a dual-hop SWIPT DF MIMO relay system with the consideration of practical imperfect CSI based on the Gaussian–Kronecker model.
2) The works carried out in this article extend the existing work [15] from the special case, where the channel correlation matrices are assumed as scaled identity matrices to scenarios with general channel correlation matrices.
3) We introduce the constant–linear–constant (CLC) nonlinear EH model [21] for the energy harvested at the relay node. The CLC-based nonlinear EH model is not considered in the existing works [14] and [15].
4) The algorithm proposed for the transceiver design in this article provides robustness to combat the inevitable channel mismatch between the exact and estimated CSI in practical scenarios. The proposed algorithm helps to improve the system performance of the existing transceiver design under a similar system model [10].
5) In this article, we consider both the fixed power constraint and the flexible power constraint at the source node. For each of the two constraints, we derive the optimal structure of the source and relay precoding matrices, which simplifies the optimization problems.
6) For the fixed power constraint, with any given TS factor, the problem is converted to two simple power allocation subproblems, while for the flexible power constraint, the problem is converted to one master problem with two associated simple power allocation subproblems, which greatly reduces the computation complexity of the optimization problem.

The remainder of this article is organized as follows. In Section II, the system model of a dual-hop MIMO relay system with an EH relayy adopting the TS protocol and consideration of the CSI mismatch is presented. In Section III, the robust transceiver design algorithm is developed with a fixed transmission power scheme at the source node. In Section IV, the robust transceiver design algorithm is developed with a flexible transmission power scheme at the source node. In Section V, the peak power limits for the source node and the relay node are considered in the optimization problem. Numerical results are presented in Section VI. Section VII concludes this article.

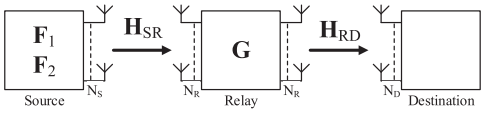

Fig. 1. Block diagram of a dual-hop MIMO relay system with EH relay using the TS protocol.

II. System Model

In this article, we consider a dual-hop three-node MIMO relay communication system, where information signals are transmitted from the source node to the destination node with the help of a relay node, as displayed in Fig. 1. The number of antennas installed at the source, relay, and destination nodes are denoted as N_S, N_R, and N_D, respectively. The source node has individual power supply, while the relay node is required to be powered by energy harvested from the received RF signals. We also assume that the direct link between the source and destination nodes is negligible due to severe pathloss and shadowing. Compared with the AF relaying scheme, we select the DF relaying scheme for the relay as it does not amplify and forward the noise introduced at the relay node.

For the EH scheme at the relay node, the TS protocol is adopted to the system. In one communication cycle, the total time T is divided into three time frames. During the first time frame of αT, the source node transmits the energy-bearing signal vector $\mathbf{s}_1 \in \mathbb{C}^{N_S \times 1}$ to the relay node for EH, where $\alpha \in [0, 1]$ represents the TS factor and the covariance matrix of $\mathbf{s}_1$ is given as $E\{\mathbf{s}_1\mathbf{s}_1^H\} = \mathbf{F}_1$, where $E\{\cdot\}$ and $(\cdot)^H$ denote the statistical expectation and Hermitian transpose, respectively. During the second time frame of $(1-\alpha)T/2$, the source node transmits information-bearing signal vector $\mathbf{s}_2 \in \mathbb{C}^{N_S \times 1}$ with covariance matrix given as $E\{\mathbf{s}_2\mathbf{s}_2^H\} = \mathbf{F}_2$ to the relay node for ID, where the relay node decodes and re-encodes the received signal. During the final time frame of $(1-\alpha)T/2$, the relay node forwards the encoded signal $\bar{\mathbf{s}} \in \mathbb{C}^{N_R \times 1}$ to the destination node,[1] where $\bar{\mathbf{s}}$ has the covariance matrix given as $E\{\bar{\mathbf{s}}\bar{\mathbf{s}}^H\} = \mathbf{G}$. For simplicity, we set $T = 1$.

The received signal at the relay node for EH during the first time frame is given as

$$\mathbf{y}_{r,1} = \mathbf{H}_{\text{SR}}\mathbf{s}_1 + \mathbf{n}_{r,1} \tag{1}$$

where $\mathbf{H}_{\text{SR}}$ is the MIMO channel matrix of the source–relay link and $\mathbf{n}_{r,1}$ is the additive white Gaussian noise (AWGN) at the relay node during the first time frame. In this article, the energy harvested at the relay node is modeled based on the CLC nonlinear EH model [21]. The RF energy $\bar{E}_r$ harvested at the relay node is written as

$$\bar{E}_r = \alpha \bar{E}_{\text{clc}}\big(\text{tr}\left\{\mathbf{H}_{\text{SR}}\mathbf{F}_1\mathbf{H}_{\text{SR}}^H\right\}\big) \tag{2}$$

where $\bar{E}_{\text{clc}}(x)$ is a piecewise function given as

$$\bar{E}_{\text{clc}}(x) = \begin{cases} 0, & x \le P_{\text{Th}} \\ E_m, & \eta_a x \ge E_m \\ \eta_a x, & \text{otherwise} \end{cases} \tag{3}$$

$\eta_a \in (0, 1)$, P_{Th}, and E_m denote the conversion efficiency at the relay node, the minimum input power, and the maximum output power of a practical EH circuit, respectively, and $\text{tr}\{\cdot\}$ denotes the matrix trace. Note that compared with the signal component, the contribution of the noise component in (1) to the energy harvested at the relay node is negligible, as pointed out in [1].

During the second time frame, the received signal at the relay node for ID is given as

$$\mathbf{y}_{r,2} = \mathbf{H}_{\text{SR}}\mathbf{s}_2 + \mathbf{n}_{r,2} \tag{4}$$

where $\mathbf{n}_{r,2}$ is the AWGN noise at the relay node with a covariance matrix of $\sigma_r^2\mathbf{I}_{N_R}$ and $\mathbf{I}_n$ denotes an $n \times n$ identity matrix. During the final time frame, the relay node forwards the re-encoded information to the destination node. The received signal at the destination node is given as

$$\mathbf{y}_d = \mathbf{H}_{\text{RD}}\bar{\mathbf{s}} + \mathbf{n}_d \tag{5}$$

where $\mathbf{H}_{\text{RD}}$ is the MIMO channel matrix of the relay–destination link and $\mathbf{n}_d$ is the AWGN noise at the destination node with a covariance matrix of $\sigma_d^2\mathbf{I}_{N_D}$.

In existing works [5]–[8], [10], [11], the exact CSI is assumed to be known at the relay and destination nodes. However, the exact CSI is unavailable in practical scenarios due to the channel estimation error, which results in mismatch between the exact and estimated CSI. Thus, the true MIMO channel matrices with the consideration of imperfect CSI are given as

$$\mathbf{H}_{\text{SR}} = \widehat{\mathbf{H}}_{\text{SR}} + \mathbf{\Delta}_{\text{SR}}, \qquad \mathbf{H}_{\text{RD}} = \widehat{\mathbf{H}}_{\text{RD}} + \mathbf{\Delta}_{\text{RD}} \tag{6}$$

where $\widehat{\mathbf{H}}_{\text{SR}}$ and $\widehat{\mathbf{H}}_{\text{RD}}$ are the estimated channel matrices for the source–relay link and the relay–destination link, respectively, $\mathbf{\Delta}_{\text{SR}}$ and $\mathbf{\Delta}_{\text{RD}}$ are the corresponding CSI mismatch matrices. It can be shown following [19] and [20] that, in general, $\mathbf{\Delta}_{\text{SR}}$ can be equivalently expressed as $\mathbf{\Sigma}_{\text{SR}}^{\frac{1}{2}}\mathbf{\Delta}_{\omega_{\text{SR}}}\mathbf{\Phi}_{\text{SR}}^{\frac{1}{2}}$, where $\mathbf{\Delta}_{\omega_{\text{SR}}}$ is an $N_R \times N_S$ complex Gaussian matrix whose entries are independent and identically distributed (i.i.d.) with zero mean and unit variance, and $\mathbf{\Sigma}_{\text{SR}}$ and $\mathbf{\Phi}_{\text{SR}}$ are the row and column covariance matrices of $\mathbf{\Delta}_{\text{SR}}$, respectively. Similarly, $\mathbf{\Delta}_{\text{RD}}$ can be equivalently expressed as $\mathbf{\Sigma}_{\text{RD}}^{\frac{1}{2}}\mathbf{\Delta}_{\omega_{\text{RD}}}\mathbf{\Phi}_{\text{RD}}^{\frac{1}{2}}$, where $\mathbf{\Sigma}_{\text{RD}}$ and $\mathbf{\Phi}_{\text{RD}}$ are the row and column covariance matrices of $\mathbf{\Delta}_{\text{RD}}$, respectively, and $\mathbf{\Delta}_{\omega_{\text{RD}}}$ is an $N_D \times N_R$ complex Gaussian matrix whose entries are i.i.d. with zero mean and unit variance. Thus, $\mathbf{\Delta}_{\text{SR}}$ and $\mathbf{\Delta}_{\text{RD}}$ follow the Gaussian–Kronecker model [20][2]

$$\mathbf{\Delta}_{\text{SR}} \sim \mathcal{CN}(\mathbf{0}, \mathbf{\Sigma}_{\text{SR}} \otimes \mathbf{\Phi}_{\text{SR}}^T) \tag{7}$$

$$\mathbf{\Delta}_{\text{RD}} \sim \mathcal{CN}(\mathbf{0}, \mathbf{\Sigma}_{\text{RD}} \otimes \mathbf{\Phi}_{\text{RD}}^T) \tag{8}$$

where $\otimes$ denotes the matrix Kronecker product and $(\cdot)^T$ stands for the matrix transpose. As pointed out in [20], in general, the

[1]It is shown in [22] that for dual-hop DF relay systems with the perfect CSI knowledge, optimizing the time allocation between the two hops of information transmission can increase the achievable system MI. However, for systems with imperfect CSI, the resulting transceiver optimization problems are intractable. Thus, we choose equal time duration for the two hops of information transmission.

[2]The methods developed in this article can be extended to other models, where the CSI mismatch matrices are Gaussian and their covariance matrices are known.

expressions of $\mathbf{\Sigma}_{\text{SR}}$, $\mathbf{\Phi}_{\text{SR}}$, $\mathbf{\Sigma}_{\text{RD}}$, and $\mathbf{\Phi}_{\text{RD}}$ depend on specific channel estimation algorithms.

The MI across the source–destination link $\mathcal{I}_{\text{SD}}$ is the minimum of the MI across the source–relay link $\mathcal{I}_{\text{SR}}$ and the MI across the relay–destination link $\mathcal{I}_{\text{RD}}$ and can be expressed as [23]

$$\mathcal{I}_{\text{SD}} = \min\left(\mathcal{I}_{\text{SR}}, \mathcal{I}_{\text{RD}}\right). \tag{9}$$

When the exact CSI is available, $\mathcal{I}_{\text{SR}}$ and $\mathcal{I}_{\text{RD}}$ are given by

$$\mathcal{I}_{\text{SR}} = \frac{1-\alpha}{2}\log_2\left|\mathbf{I}_{N_R} + \sigma_r^{-2}\mathbf{H}_{\text{SR}}\mathbf{F}_2\mathbf{H}_{\text{SR}}^H\right| \tag{10}$$

$$\mathcal{I}_{\text{RD}} = \frac{1-\alpha}{2}\log_2\left|\mathbf{I}_{N_D} + \sigma_d^{-2}\mathbf{H}_{\text{RD}}\mathbf{G}\mathbf{H}_{\text{RD}}^H\right| \tag{11}$$

where $|\cdot|$ denotes the matrix determinant. With the consideration of the CSI mismatch, it is noted that the exact $\mathcal{I}_{\text{SR}}$ and $\mathcal{I}_{\text{RD}}$ are unknown [19], [24]–[26]. Based on [19] and [24]–[26], we adopt the lower bound of the exact $\mathcal{I}_{\text{SR}}$ and $\mathcal{I}_{\text{RD}}$ in this article, which can be written as

$$\tilde{\mathcal{I}}_{\text{SR}} = \frac{1-\alpha}{2}\log_2\left|\mathbf{I}_{N_R} + \mathbf{T}_{\text{SR}}^{-\frac{1}{2}}\widehat{\mathbf{H}}_{\text{SR}}\mathbf{F}_2\widehat{\mathbf{H}}_{\text{SR}}^H\mathbf{T}_{\text{SR}}^{-\frac{H}{2}}\right| \tag{12}$$

$$\tilde{\mathcal{I}}_{\text{RD}} = \frac{1-\alpha}{2}\log_2\left|\mathbf{I}_{N_D} + \mathbf{T}_{\text{RD}}^{-\frac{1}{2}}\widehat{\mathbf{H}}_{\text{RD}}\mathbf{G}\widehat{\mathbf{H}}_{\text{RD}}^H\mathbf{T}_{\text{RD}}^{-\frac{H}{2}}\right| \tag{13}$$

where $(\cdot)^{-1}$ denotes the matrix inversion and

$$\begin{aligned}\mathbf{T}_{\text{SR}} &= \sigma_r^2\mathbf{I}_{N_R} + E\{\mathbf{\Delta}_{\text{SR}}\mathbf{F}_2\mathbf{\Delta}_{\text{SR}}^H\}\\ &= \sigma_r^2\mathbf{I}_{N_R} + \text{tr}\{\mathbf{F}_2\mathbf{\Phi}_{\text{SR}}\}\mathbf{\Sigma}_{\text{SR}} \qquad (14)\\ \mathbf{T}_{\text{RD}} &= \sigma_d^2\mathbf{I}_{N_D} + E\{\mathbf{\Delta}_{\text{RD}}\mathbf{G}\mathbf{\Delta}_{\text{RD}}^H\}\\ &= \sigma_d^2\mathbf{I}_{N_D} + \text{tr}\{\mathbf{G}\mathbf{\Phi}_{\text{RD}}\}\mathbf{\Sigma}_{\text{RD}} \qquad (15)\end{aligned}$$

are the equivalent noise covariance matrices. It can be seen that when the CSI is nonideal and the channel estimation errors $\mathbf{\Delta}_{\text{SR}}$ and $\mathbf{\Delta}_{\text{RD}}$ follow the Gaussian–Kronecker model, the system MI lower bounds (12) and (13) are different to the conventional system MI (10) and (11) due to the existence of $\mathbf{T}_{\text{SR}}$ and $\mathbf{T}_{\text{RD}}$, which are not identity matrices. Moreover, with the consideration of the CSI mismatch, $\bar{E}_r$ from (2) is rewritten into

$$\begin{aligned}\tilde{E}_r &= \alpha\bar{E}_{\text{clc}}\left(E\{(\widehat{\mathbf{H}}_{\text{SR}} + \mathbf{\Delta}_{\text{SR}})\mathbf{F}_1(\widehat{\mathbf{H}}_{\text{SR}} + \mathbf{\Delta}_{\text{SR}})^H\}\right)\\ &= \alpha\bar{E}_{\text{clc}}\left(\text{tr}\{\mathbf{F}_1(\widehat{\mathbf{H}}_{\text{SR}}^H\widehat{\mathbf{H}}_{\text{SR}} + \text{tr}\{\mathbf{\Sigma}_{\text{SR}}\}\mathbf{\Phi}_{\text{SR}})\}\right). \qquad (16)\end{aligned}$$

In the TS protocol, there are two schemes of transmission power constraint for the source node [1], which are known as the fixed power scheme and the flexible power scheme. The transmission power constraint for the source node in the case of the fixed power scheme is given as

$$\text{tr}\{\mathbf{F}_1\} \le P_s, \quad \text{tr}\{\mathbf{F}_2\} \le P_s \tag{17}$$

and that in the case of the flexible power scheme is given by

$$\alpha\,\text{tr}\{\mathbf{F}_1\} + \frac{1-\alpha}{2}\text{tr}\{\mathbf{F}_2\} \le \frac{1+\alpha}{2}P_s \tag{18}$$

where $P_s > 0$ is the power budget available at the source node.

The energy consumption at the relay node consists of the transmission energy and the circuit energy [27]. The amount of energy used to transmit $\bar{\mathbf{s}}$ to the destination node is given by $\frac{1-\alpha}{2}\text{tr}\{\mathbf{G}\}$. Based on [10], the amount of energy used to maintain the circuit operations at the relay node consists of a static part that is given as $\frac{1-\alpha}{2}N_RP_c$ and a dynamic part that is modeled as $\eta_b\tilde{E}_r$, where P_c is the per-antenna static power consumption and $\eta_b \in (0,1)$. It has been shown in [7] that the achievable data rate increases with $\tilde{E}_r$. As the amount of information processing at the relay node increases with the data rate, it is sensible to adopt $\eta_b\tilde{E}_r$ as the dynamic part of the circuit energy consumption. Hence, the energy consumption constraint at the relay node is written as

$$\frac{1-\alpha}{2}\left(\text{tr}\{\mathbf{G}\} + N_RP_c\right) \le E_r \tag{19}$$

where $E_r = \alpha E_{\text{clc}}(\text{tr}\{\mathbf{F}_1(\widehat{\mathbf{H}}_{\text{SR}}^H\widehat{\mathbf{H}}_{\text{SR}} + \text{tr}\{\mathbf{\Sigma}_{\text{SR}}\}\mathbf{\Phi}_{\text{SR}})\})$, $E_{\text{clc}}(x)$ is given as

$$E_{\text{clc}}(x) = \begin{cases} 0, & x \le P_{\text{Th}} \\ E_m, & \eta x \ge E_m \\ \eta x, & \text{otherwise}\end{cases} \tag{20}$$

and $\eta = \eta_a(1-\eta_b)$.

The main objective of the proposed transceiver design scheme is to maximize $\mathcal{I}_{\text{SD,low}} = \min(\tilde{\mathcal{I}}_{\text{SR}}, \tilde{\mathcal{I}}_{\text{RD}})$ subjecting to each variation of transmission power constraints at the source node, as given in (17) and (18), and the energy consumption constraint at the relay node, as given by (19).

Different from [15], the CSI mismatch covariance matrices $\mathbf{\Phi}_{\text{SR}}$, $\mathbf{\Phi}_{\text{RD}}$, $\mathbf{\Sigma}_{\text{SR}}$, and $\mathbf{\Sigma}_{\text{RD}}$ in general cases are not scaled identity matrices, which result in difficulties when solving the optimization problem. In general cases, where $\mathbf{\Phi}_{\text{SR}} \neq \sigma_e^2\mathbf{I}_{N_S}$ and $\mathbf{\Phi}_{\text{RD}} \neq \sigma_e^2\mathbf{I}_{N_R}$, we introduce the following inequality [20] to overcome the challenge:

$$\text{tr}\{\mathbf{AB}\} \le \text{tr}\{\mathbf{A}\}\lambda_M(\mathbf{B}) \tag{21}$$

where $\lambda_M(\cdot)$ denotes the maximal eigenvalue of a matrix. By applying (21) to (14) and (15), the upper bound of $\mathbf{T}_{\text{SR}}$ and $\mathbf{T}_{\text{RD}}$, which are, respectively, denoted as $\hat{\mathbf{T}}_{\text{SR}}$ and $\hat{\mathbf{T}}_{\text{RD}}$, are given as

$$\hat{\mathbf{T}}_{\text{SR}} = \sigma_r^2\mathbf{I}_{N_R} + \text{tr}\{\mathbf{F}_2\}\varphi_{\text{SR}}\mathbf{\Sigma}_{\text{SR}} \tag{22}$$

$$\hat{\mathbf{T}}_{\text{RD}} = \sigma_d^2\mathbf{I}_{N_D} + \text{tr}\{\mathbf{G}\}\varphi_{\text{RD}}\mathbf{\Sigma}_{\text{RD}} \tag{23}$$

where φ_{SR} and φ_{RD} denote the maximal eigenvalue of $\mathbf{\Phi}_{\text{SR}}$ and $\mathbf{\Phi}_{\text{RD}}$, respectively. Notably, (22) and (23) are also applicable in the case, where $\mathbf{\Phi}_{\text{SR}} = \sigma_e^2\mathbf{I}_{N_S}$ and $\mathbf{\Phi}_{\text{RD}} = \sigma_e^2\mathbf{I}_{N_R}$. By substituting (22) and (23) into (12) and (13), we obtain the lower bound of $\mathcal{I}_{\text{SD}}$, denoted as $\hat{\mathcal{I}}_{\text{SD}} = \min(\hat{\mathcal{I}}_{\text{SR}}, \hat{\mathcal{I}}_{\text{RD}})$, where $\hat{\mathcal{I}}_{\text{SR}}$ and $\hat{\mathcal{I}}_{\text{RD}}$ represent the lower bounds of $\tilde{\mathcal{I}}_{\text{SR}}$ and $\tilde{\mathcal{I}}_{\text{RD}}$, respectively, given by

$$\hat{\mathcal{I}}_{\text{SR}} = \frac{1-\alpha}{2}\log_2\left|\mathbf{I}_{N_R} + \hat{\mathbf{T}}_{\text{SR}}^{-\frac{1}{2}}\widehat{\mathbf{H}}_{\text{SR}}\mathbf{F}_2\widehat{\mathbf{H}}_{\text{SR}}^H\hat{\mathbf{T}}_{\text{SR}}^{-\frac{H}{2}}\right| \tag{24}$$

$$\hat{\mathcal{I}}_{\text{RD}} = \frac{1-\alpha}{2}\log_2\left|\mathbf{I}_{N_D} + \hat{\mathbf{T}}_{\text{RD}}^{-\frac{1}{2}}\widehat{\mathbf{H}}_{\text{RD}}\mathbf{G}\widehat{\mathbf{H}}_{\text{RD}}^H\hat{\mathbf{T}}_{\text{RD}}^{-\frac{H}{2}}\right|. \tag{25}$$

In this article, we optimize the system parameters to maximize $\hat{\mathcal{I}}_{\text{SD}}$.

In general cases, where $\mathbf{\Sigma}_{\text{SR}} \neq \sigma_e^2\mathbf{I}_{N_R}$ and $\mathbf{\Sigma}_{\text{RD}} \neq \sigma_e^2\mathbf{I}_{N_D}$, the eigenvalue decomposition (EVD) of $\mathbf{\Sigma}_{\text{SR}}$ and $\mathbf{\Sigma}_{\text{RD}}$ is introduced to reduce the complexity of the objective function as follows:

$$\mathbf{\Sigma}_{\text{SR}} = \mathbf{V}_{\Sigma_{\text{SR}}}\mathbf{\Lambda}_{\Sigma_{\text{SR}}}\mathbf{V}_{\Sigma_{\text{SR}}}^H, \ \mathbf{\Sigma}_{\text{RD}} = \mathbf{V}_{\Sigma_{\text{RD}}}\mathbf{\Lambda}_{\Sigma_{\text{RD}}}\mathbf{V}_{\Sigma_{\text{RD}}}^H. \tag{26}$$

With the introduction of (26), $\hat{\mathcal{I}}_{\text{SR}}$ and $\hat{\mathcal{I}}_{\text{RD}}$ in (24) and (25) are equivalently rewritten into

$$\hat{\mathcal{I}}_{\text{SR}} = \frac{1-\alpha}{2}\log_2\left|\mathbf{I}_{N_R}+\widetilde{\mathbf{H}}_{\text{SR}}[\text{tr}\{\mathbf{F}_2\}]\mathbf{F}_2\widetilde{\mathbf{H}}_{\text{SR}}^H[\text{tr}\{\mathbf{F}_2\}]\right| \quad (27)$$

$$\hat{\mathcal{I}}_{\text{RD}} = \frac{1-\alpha}{2}\log_2\left|\mathbf{I}_{N_D}+\widetilde{\mathbf{H}}_{\text{RD}}[\text{tr}\{\mathbf{G}\}]\mathbf{G}\widetilde{\mathbf{H}}_{\text{RD}}^H[\text{tr}\{\mathbf{G}\}]\right| \quad (28)$$

where

$$\widetilde{\mathbf{H}}_{\text{SR}}[\text{tr}\{\mathbf{F}_2\}] = \left(\sigma_r^2\mathbf{I}_{N_R}+\text{tr}\{\mathbf{F}_2\}\varphi_{\text{SR}}\mathbf{\Lambda}_{\Sigma_{\text{SR}}}\right)^{-\frac{1}{2}}\mathbf{V}_{\Sigma_{\text{SR}}}^H\widehat{\mathbf{H}}_{\text{SR}}$$

$$\widetilde{\mathbf{H}}_{\text{RD}}[\text{tr}\{\mathbf{G}\}] = \left(\sigma_d^2\mathbf{I}_{N_D}+\text{tr}\{\mathbf{G}\}\varphi_{\text{RD}}\mathbf{\Lambda}_{\Sigma_{\text{RD}}}\right)^{-\frac{1}{2}}\mathbf{V}_{\Sigma_{\text{RD}}}^H\widehat{\mathbf{H}}_{\text{RD}}$$

can be viewed as the source–relay link channel matrix with dependence on $\text{tr}\{\mathbf{F}_2\}$ and the relay–destination link channel matrix with dependence on $\text{tr}\{\mathbf{G}\}$, respectively, with the corresponding compact singular value decomposition (SVD) given as

$$\widetilde{\mathbf{H}}_{\text{SR}}[\text{tr}\{\mathbf{F}_2\}] = \widetilde{\mathbf{U}}_{\text{SR}}[\text{tr}\{\mathbf{F}_2\}]\widetilde{\mathbf{\Lambda}}_{\text{SR}}^{\frac{1}{2}}[\text{tr}\{\mathbf{F}_2\}]\widetilde{\mathbf{V}}_{\text{SR}}^H[\text{tr}\{\mathbf{F}_2\}] \quad (29)$$

$$\widetilde{\mathbf{H}}_{\text{RD}}[\text{tr}\{\mathbf{G}\}] = \widetilde{\mathbf{U}}_{\text{RD}}[\text{tr}\{\mathbf{G}\}]\widetilde{\mathbf{\Lambda}}_{\text{RD}}^{\frac{1}{2}}[\text{tr}\{\mathbf{G}\}]\widetilde{\mathbf{V}}_{\text{RD}}^H[\text{tr}\{\mathbf{G}\}] \quad (30)$$

where $\widetilde{\mathbf{\Lambda}}_{\text{SR}}[\text{tr}\{\mathbf{F}_2\}]$ and $\widetilde{\mathbf{\Lambda}}_{\text{RD}}[\text{tr}\{\mathbf{G}\}]$ are diagonal matrices with dimension of $K_{\text{SR}} = \min(N_S, N_R)$ and $K_{\text{RD}} = \min(N_R, N_D)$, respectively, with the diagonal elements arranged in descending order.

III. Fixed Power Scheme

In this section, we investigate the optimization problem, which maximizes $\hat{\mathcal{I}}_{\text{SD}}$ with $\hat{\mathcal{I}}_{\text{SR}}$ and $\hat{\mathcal{I}}_{\text{RD}}$ expressed in (27) and (28), respectively. Subjecting to the fixed transmission power constraint as given in (17) and the energy consumption constraint as given in (19), the optimization problem can be written as

$$\max_{\alpha,\mathbf{F}_1,\mathbf{F}_2,\mathbf{G}} \hat{\mathcal{I}}_{\text{SD}} \quad (31a)$$

$$\text{s.t. } \text{tr}\{\mathbf{F}_1\} \le P_s, \quad \text{tr}\{\mathbf{F}_2\} \le P_s \quad (31b)$$

$$\frac{1-\alpha}{2}\left(\text{tr}\{\mathbf{G}\} + N_R P_c\right) \le E_r \quad (31c)$$

$$\mathbf{F}_1 \ge 0, \quad \mathbf{F}_2 \ge 0, \quad \mathbf{G} \ge 0 \quad (31d)$$

$$0 \le \alpha \le 1. \quad (31e)$$

It is noticeable that $\mathbf{F}_1$ is not involved in the objective function, but it affects the transmission energy available at the relay node. Thus, the optimization problem for $\mathbf{F}_1$ can be viewed as

$$\max_{\mathbf{F}_1} \text{tr}\{\mathbf{F}_1\mathbf{Q}\} \quad (32a)$$

$$\text{s.t. } \text{tr}\{\mathbf{F}_1\} \le P_s, \quad \mathbf{F}_1 \ge 0 \quad (32b)$$

where $\mathbf{Q} = \widehat{\mathbf{H}}_{\text{SR}}^H\widehat{\mathbf{H}}_{\text{SR}} + \text{tr}\{\mathbf{\Sigma}_{\text{SR}}\}\mathbf{\Phi}_{\text{SR}}$ with the corresponding EVD given as $\mathbf{V}_q\mathbf{\Lambda}_q\mathbf{V}_q^H$ and the diagonal elements of $\mathbf{\Lambda}_q$ are arranged in decreasing order. As the optimal $\mathbf{F}_1$ must achieve the equality of the transmission power constraint (32b), the optimal structure [5] for $\mathbf{F}_1$ is given $\mathbf{F}_1 = P_s\mathbf{v}_{q,1}\mathbf{v}_{q,1}^H$, where $\mathbf{v}_{q,1}$ is the leftmost column of $\mathbf{V}_q$. By adopting the optimal structure of $\mathbf{F}_1$, the optimization problem (31) can be rewritten as

$$\max_{\alpha,\mathbf{F}_2,\mathbf{G}} \min\left(\frac{1-\alpha}{2}\log_2\left|\mathbf{I}_{N_R}+\widetilde{\mathbf{H}}_{\text{SR}}[\text{tr}\{\mathbf{F}_2\}]\mathbf{F}_2\widetilde{\mathbf{H}}_{\text{SR}}^H[\text{tr}\{\mathbf{F}_2\}]\right|,\right.$$

$$\left.\frac{1-\alpha}{2}\log_2\left|\mathbf{I}_{N_D}+\widetilde{\mathbf{H}}_{\text{RD}}[\text{tr}\{\mathbf{G}\}]\mathbf{G}\widetilde{\mathbf{H}}_{\text{RD}}^H[\text{tr}\{\mathbf{G}\}]\right|\right) \quad (33a)$$

$$\text{s.t. } \text{tr}\{\mathbf{F}_2\} \le P_s \quad (33b)$$

$$\text{tr}\{\mathbf{G}\} \le E_\alpha \quad (33c)$$

$$0 \le \alpha \le 1, \quad \mathbf{F}_2 \ge 0, \quad \mathbf{G} \ge 0 \quad (33d)$$

where $E_\alpha = 2\alpha E_{\text{clc}}(\chi P_s)/(1-\alpha) - N_R P_c$ and χ is the largest diagonal element of $\mathbf{\Lambda}_q$.

The optimization problem (33) is solved by an iterative method. Let us denote $\hat{\mathcal{I}}_{\text{SD}}\{\alpha\}$ as the optimal $\hat{\mathcal{I}}_{\text{SD}}$ with any given α value. First, we solve the optimization problem with fixed α. It is noted that E_α is a constant with any given α. It can be shown that $\hat{\mathcal{I}}_{\text{SR}}$ in (27) is monotonically increasing with respect to $\text{tr}\{\mathbf{F}_2\}$ and $\hat{\mathcal{I}}_{\text{RD}}$ in (28) increases monotonically with respect to $\text{tr}\{\mathbf{G}\}$. Thus, it is obvious that the optimal $\mathbf{F}_2$ and $\mathbf{G}$ must achieve the equality of corresponding power constraints (33b) and (33c). Thus, under fixed transmission power constraint, $\widetilde{\mathbf{H}}_{\text{SR}}[\text{tr}\{\mathbf{F}_2\}] = \widetilde{\mathbf{H}}_{\text{SR}}[P_s]$ and $\widetilde{\mathbf{H}}_{\text{RD}}[\text{tr}\{\mathbf{G}\}] = \widetilde{\mathbf{H}}_{\text{RD}}[E_\alpha]$ can be rewritten as

$$\widetilde{\mathbf{H}}_{\text{SR}}[P_s] = \left(\sigma_r^2\mathbf{I}_{N_R} + P_s\varphi_{\text{SR}}\mathbf{\Lambda}_{\Sigma_{\text{SR}}}\right)^{-\frac{1}{2}}\mathbf{V}_{\Sigma_{\text{SR}}}^H\widehat{\mathbf{H}}_{\text{SR}}$$

$$\widetilde{\mathbf{H}}_{\text{RD}}[E_\alpha] = \left(\sigma_d^2\mathbf{I}_{N_D} + E_\alpha\varphi_{\text{RD}}\mathbf{\Lambda}_{\Sigma_{\text{RD}}}\right)^{-\frac{1}{2}}\mathbf{V}_{\Sigma_{\text{RD}}}^H\widehat{\mathbf{H}}_{\text{RD}}$$

with the corresponding compact SVD written as

$$\widetilde{\mathbf{H}}_{\text{SR}}[P_s] = \widetilde{\mathbf{U}}_{\text{SR}}\widetilde{\mathbf{\Lambda}}_{\text{SR}}^{\frac{1}{2}}[P_s]\widetilde{\mathbf{V}}_{\text{SR}}^H \quad (34)$$

$$\widetilde{\mathbf{H}}_{\text{RD}}[E_\alpha] = \widetilde{\mathbf{U}}_{\text{RD}}\widetilde{\mathbf{\Lambda}}_{\text{RD}}^{\frac{1}{2}}[E_\alpha]\widetilde{\mathbf{V}}_{\text{RD}}^H. \quad (35)$$

The diagonal elements of $\widetilde{\mathbf{\Lambda}}_{\text{SR}}[P_s]$ and $\widetilde{\mathbf{\Lambda}}_{\text{RD}}[E_\alpha]$ are arranged in descending order and the ith diagonal elements of the corresponding matrices are denoted as $\widetilde{\lambda}_{\text{SR},i}[P_s]$ for $i = 1, \ldots, K_{\text{SR}}$ and $\widetilde{\lambda}_{\text{RD},i}[E_\alpha]$ for $i = 1, \ldots, K_{\text{RD}}$. As mentioned in [12], when $\text{tr}\{\mathbf{F}_2\}$ and $\text{tr}\{\mathbf{G}\}$ are constants, $\widetilde{\mathbf{U}}_{\text{SR}}, \widetilde{\mathbf{U}}_{\text{RD}}, \widetilde{\mathbf{V}}_{\text{SR}}$, and $\widetilde{\mathbf{V}}_{\text{RD}}$ do not depend on $\mathbf{F}_2$ and $\mathbf{G}$. It can be shown that the optimal structures for $\mathbf{F}_2$ and $\mathbf{G}$ are given by

$$\mathbf{F}_2 = \widetilde{\mathbf{V}}_{\text{SR}}\mathbf{\Lambda}_2\widetilde{\mathbf{V}}_{\text{SR}}^H, \qquad \mathbf{G} = \widetilde{\mathbf{V}}_{\text{RD}}\mathbf{\Lambda}_g\widetilde{\mathbf{V}}_{\text{RD}}^H \quad (36)$$

where $\mathbf{\Lambda}_2$ and $\mathbf{\Lambda}_g$ are diagonal matrices of size K_{SR} and K_{RD}, respectively. The ith diagonal elements for $\mathbf{\Lambda}_2$ and $\mathbf{\Lambda}_g$ are correspondingly denoted as $\lambda_{2,i}$ for $i = 1, \ldots, K_{\text{SR}}$ and $\lambda_{g,i}$ for $i = 1, \ldots, K_{\text{RD}}$. By adopting the optimal structures of $\mathbf{F}_2$ and $\mathbf{G}$, the optimization problem (33) can be written as

$$\max_{\mathbf{F}_2,\mathbf{G}} \min\left(\frac{1-\alpha}{2}\log_2\left|\mathbf{I}_{N_R} + \widetilde{\mathbf{\Lambda}}_{\text{SR}}^{\frac{1}{2}}[P_s]\mathbf{\Lambda}_2\widetilde{\mathbf{\Lambda}}_{\text{SR}}^{\frac{1}{2}}[P_s]\right|,\right.$$

$$\left.\frac{1-\alpha}{2}\log_2\left|\mathbf{I}_{N_D} + \widetilde{\mathbf{\Lambda}}_{\text{RD}}^{\frac{1}{2}}[E_\alpha]\mathbf{\Lambda}_g\widetilde{\mathbf{\Lambda}}_{\text{RD}}^{\frac{1}{2}}[E_\alpha]\right|\right) \quad (37a)$$

$$\text{s.t. } \text{tr}\{\mathbf{\Lambda}_2\} \le P_s \quad (37b)$$

$$\text{tr}\{\mathbf{\Lambda}_g\} \le E_\alpha \quad (37c)$$

$$\mathbf{F}_2 \ge 0, \quad \mathbf{G} \ge 0. \quad (37d)$$

As the optimization problem (37) contains only diagonalized matrix, it can be simplified to a power allocation problem with

scalar variables, which is given as

$$\max_{\boldsymbol{\lambda}_2,\boldsymbol{\lambda}_g} \min \left(\frac{1-\alpha}{2} \sum_{i=1}^{K_{\mathrm{SR}}} \log_2 \left(1+\widetilde{\lambda}_{\mathrm{SR},i}[P_s]\lambda_{2,i}\right), \right.$$
$$\left. \frac{1-\alpha}{2} \sum_{i=1}^{K_{\mathrm{RD}}} \log_2 \left(1+\widetilde{\lambda}_{\mathrm{RD},i}[E_\alpha]\lambda_{g,i}\right) \right) \quad (38a)$$

$$\text{s.t.} \sum_{i=1}^{K_{\mathrm{SR}}} \lambda_{2,i} \le P_s, \quad \lambda_{2,i} \ge 0, \qquad i=1,\ldots,K_{\mathrm{SR}} \quad (38b)$$

$$\sum_{i=1}^{K_{\mathrm{RD}}} \lambda_{g,i} \le E_\alpha, \quad \lambda_{g,i} \ge 0, \qquad i=1,\ldots,K_{\mathrm{RD}} \quad (38c)$$

where $\boldsymbol{\lambda}_2 = [\lambda_{2,1},\ldots,\lambda_{2,K_{\mathrm{SR}}}]^T$ and $\boldsymbol{\lambda}_g = [\lambda_{g,1},\ldots,\lambda_{g,K_{\mathrm{RD}}}]^T$. It is noted that (38a) can be further reduced to two subproblems. In particular, the source–relay link optimization problem is given as

$$\max_{\boldsymbol{\lambda}_2} \frac{1-\alpha}{2} \sum_{i=1}^{K_{\mathrm{SR}}} \log_2 \left(1+\widetilde{\lambda}_{\mathrm{SR},i}[P_s]\lambda_{2,i}\right) \quad (39a)$$

$$\text{s.t.} \sum_{i=1}^{K_{\mathrm{SR}}} \lambda_{2,i} \le P_s, \quad \lambda_{2,i} \ge 0, \qquad i=1,\ldots,K_{\mathrm{SR}} \quad (39b)$$

while the relay–destination link optimization problem is given as

$$\max_{\boldsymbol{\lambda}_g} \frac{1-\alpha}{2} \sum_{i=1}^{K_{\mathrm{RD}}} \log_2 \left(1+\widetilde{\lambda}_{\mathrm{RD},i}[E_\alpha]\lambda_{g,i}\right) \quad (40a)$$

$$\text{s.t.} \sum_{i=1}^{K_{\mathrm{RD}}} \lambda_{g,i} \le E_\alpha, \quad \lambda_{g,i} \ge 0, \qquad i=1,\ldots,K_{\mathrm{RD}}. \quad (40b)$$

By using the Karush–Kuhn–Tucker (KKT) conditions, the optimal $\lambda_{2,i}$ is given as

$$\lambda_{2,i}^* = \frac{1}{\widetilde{\lambda}_{\mathrm{SR},i}[P_s]} \left[\frac{1-\alpha}{2} \frac{\widetilde{\lambda}_{\mathrm{SR},i}[P_s]}{\mu_1 \ln 2} - 1 \right]^+, \quad i=1,\ldots,K_{\mathrm{SR}} \quad (41)$$

and the optimal $\lambda_{g,i}$ is written as

$$\lambda_{g,i}^* = \frac{1}{\widetilde{\lambda}_{\mathrm{RD},i}[E_\alpha]} \left[\frac{1-\alpha}{2} \frac{\widetilde{\lambda}_{\mathrm{RD},i}[E_\alpha]}{\mu_2 \ln 2} - 1 \right]^+, \quad i=1,\ldots,K_{\mathrm{RD}} \quad (42)$$

where $(\cdot)^*$ represents the optimal value, $\ln$ denotes the natural logarithm, $[x]^+ = \max(x,0)$, and $\mu_1 > 0$ and $\mu_2 > 0$ are the Lagrange multipliers to (39b) and (40b), respectively.

It can be seen that the objective function $\hat{\mathcal{I}}_{\mathrm{SD}}$ for fixed transmission power constraint is a unimodal function of α, as illustrated in Fig. 2, and the feasibility region of (33c) is monotonically increasing with α. Thus, the optimal α can be obtained through the golden section search method with the golden number ratio $\delta = 1.618$ [28]. The procedure of the golden section search method is presented in Algorithm 1, where $\varepsilon > 0$ is a small number controlling the convergence of the algorithm.

The transceiver optimization problems are solved at the source node since it has constant power supply. The value of α does not need to be sent to the relay nor the destination, as the relay node is able to tell whether the incoming signal is energy-bearing signal $\mathbf{s}_1$ or information-carrying signal $\mathbf{s}_2$ through the property/structure of $\mathbf{s}_1$ and $\mathbf{s}_2$.

Algorithm 1: Golden Section Search Method to Find the Optimal α.

Initialization: $\alpha_U = 1$ and $\alpha_L = 0$.
while $|\alpha_U - \alpha_L| \ge \varepsilon$ **do**
  Set $\rho_1 = (\delta-1)\alpha_L + (2-\delta)\alpha_U$.
  Set $\rho_2 = (2-\delta)\alpha_L + (\delta-1)\alpha_U$.
  Compute $\hat{\mathcal{I}}_{\mathrm{SD}}\{\rho_1\}$ and $\hat{\mathcal{I}}_{\mathrm{SD}}\{\rho_2\}$.
  if $\hat{\mathcal{I}}_{\mathrm{SD}}\{\rho_1\} - \hat{\mathcal{I}}_{\mathrm{SD}}\{\rho_2\} \ge 0$ **then**
    $\alpha_U = \rho_2$.
  else
    $\alpha_L = \rho_1$.
  end if
end while
$\alpha^* = (\alpha_L + \alpha_U)/2$.

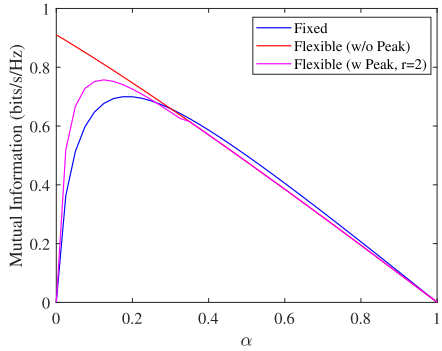

Fig. 2. Unimodality of $\mathcal{I}_{\mathrm{SD}}$; $P_s = 20$ dBm and $N_S = N_R = N_D = 2$.

IV. Flexible Power Scheme

In this section, we investigate the optimization problem, which maximizes $\hat{\mathcal{I}}_{\mathrm{SD}}$ with $\hat{\mathcal{I}}_{\mathrm{SR}}$ and $\hat{\mathcal{I}}_{\mathrm{RD}}$ expressed in (27) and (28) respectively. Subjecting to the flexible power constraint as given in (18) and the energy consumption constraint as given in (19), the optimization problem can be expressed as

$$\max_{\alpha,\mathbf{F}_1,\mathbf{F}_2,\mathbf{G}} \hat{\mathcal{I}}_{\mathrm{SD}} \quad (43a)$$

$$\text{s.t. } \alpha \mathrm{tr}\{\mathbf{F}_1\} + \frac{1-\alpha}{2}\mathrm{tr}\{\mathbf{F}_2\} \le \frac{1+\alpha}{2} P_s \quad (43b)$$

$$\frac{1-\alpha}{2}\left(\mathrm{tr}\{\mathbf{G}\} + N_R P_c\right) \le E_r \quad (43c)$$

$$\mathbf{F}_1 \ge 0, \quad \mathbf{F}_2 \ge 0, \quad \mathbf{G} \ge 0 \quad (43d)$$

$$0 \le \alpha \le 1. \quad (43e)$$

It is noticeable that the optimal $\mathbf{F}_1$ is not involved in the objective function (43a), but it affects the objective function by varying the feasible region of the problem. To maximize the energy harvested at the relay node, the source node transmission power for the energy-carrying signal should be located to the strongest subchannel of $\mathbf{Q}$. By assuming that $\mathrm{tr}\{\mathbf{F}_1\} = \lambda_1$, the

optimization of $\mathbf{F}_1$ can be reduced to λ_1 with the optimal structure for $\mathbf{F}_1 = \lambda_1 \mathbf{v}_{q,1}\mathbf{v}_{q,1}^H$. By adopting the optimal structure of $\mathbf{F}_1$, the optimization problem (43) is rewritten as

$$\max_{\alpha,\lambda_1,\mathbf{F}_2,\mathbf{G}} \hat{\mathcal{I}}_{\text{SD}} \tag{44a}$$

$$\text{s.t. } \alpha\lambda_1 + \frac{1-\alpha}{2}\text{tr}\{\mathbf{F}_2\} \le \frac{1+\alpha}{2}P_s \tag{44b}$$

$$\text{tr}\{\mathbf{G}\} \le \frac{2\alpha}{1-\alpha}E_{\text{clc}}(\lambda_1\chi) - N_R P_c \tag{44c}$$

$$\lambda_1 \ge 0, 0 \le \alpha \le 1, \ \ \mathbf{F}_2 \ge 0, \ \ \mathbf{G} \ge 0. \tag{44d}$$

Similar to Section III, an iterative method is developed to solve the problem (44). It is noticed that the optimal $\mathbf{F}_2$ and $\mathbf{G}$ are coupled by λ_1 with any given α. The primal decomposition method is applied by introducing $\alpha\lambda_1 = k$, where $k \in [0, \frac{1+\alpha}{2}P_s]$. The optimization problem (44) is equivalently decomposed into two subproblems, which are written as

$$\max_{\mathbf{F}_2} \ \ \hat{\mathcal{I}}_{\text{SR}}(k) = \frac{1-\alpha}{2}\log_2\left|\mathbf{I}_{N_R} + \widetilde{\mathbf{H}}_{\text{SR}}[\text{tr}\{\mathbf{F}_2\}]\mathbf{F}_2\widetilde{\mathbf{H}}_{\text{SR}}^H[\text{tr}\{\mathbf{F}_2\}]\right| \tag{45a}$$

$$\text{s.t. } \text{tr}\{\mathbf{F}_2\} \le P_f, \ \ \mathbf{F}_2 \ge 0 \tag{45b}$$

and

$$\max_{\mathbf{G}} \ \ \hat{\mathcal{I}}_{\text{RD}}(k) = \frac{1-\alpha}{2}\log_2\left|\mathbf{I}_{N_D} + \widetilde{\mathbf{H}}_{\text{RD}}[\text{tr}\{\mathbf{G}\}]\mathbf{G}\widetilde{\mathbf{H}}_{\text{RD}}^H[\text{tr}\{\mathbf{G}\}]\right| \tag{46a}$$

$$\text{s.t. } \text{tr}\{\mathbf{G}\} \le E_f, \ \ \mathbf{G} \ge 0 \tag{46b}$$

where

$$P_f = \frac{(1+\alpha)P_s - 2\,k}{1-\alpha}, E_f = \frac{2\alpha}{1-\alpha}E_{\text{clc}}\left(\frac{k}{\alpha}\chi\right) - N_R P_c \tag{47}$$

and $\hat{\mathcal{I}}_{\text{SR}}(k)$ and $\hat{\mathcal{I}}_{\text{RD}}(k)$ are the optimal $\hat{\mathcal{I}}_{\text{SR}}$ and $\hat{\mathcal{I}}_{\text{RD}}$ with a given k. Moreover, the master problem of optimizing $\mathbf{F}_2$ and $\mathbf{G}$ is given as

$$\max_{k} \min(\hat{\mathcal{I}}_{\text{SR}}(k), \hat{\mathcal{I}}_{\text{RD}}(k)) \tag{48a}$$

$$\text{s.t. } 0 \le k \le \frac{(1+\alpha)P_s}{2}. \tag{48b}$$

It can be easily seen that the equality of (45b) and (46b) must be achieved with the optimal $\mathbf{F}_2$ for the problem (45a) and $\mathbf{G}$ for the problem (46a). Thus, $\widetilde{\mathbf{H}}_{\text{SR}}[\text{tr}\{\mathbf{F}_2\}] = \widetilde{\mathbf{H}}_{\text{SR}}[P_f]$ and $\widetilde{\mathbf{H}}_{\text{RD}}[\text{tr}\{\mathbf{G}\}] = \widetilde{\mathbf{H}}_{\text{RD}}[E_f]$ can be rewritten as

$$\widetilde{\mathbf{H}}_{\text{SR}}[P_f] = \left(\sigma_r^2\mathbf{I}_{N_R} + P_f\varphi_{\text{SR}}\mathbf{\Lambda}_{\Sigma_{\text{SR}}}\right)^{-\frac{1}{2}}\mathbf{V}_{\Sigma_{\text{SR}}}^H\widehat{\mathbf{H}}_{\text{SR}}$$

$$\widetilde{\mathbf{H}}_{\text{RD}}[E_f] = \left(\sigma_d^2\mathbf{I}_{N_D} + E_f\varphi_{\text{RD}}\mathbf{\Lambda}_{\Sigma_{\text{RD}}}\right)^{-\frac{1}{2}}\mathbf{V}_{\Sigma_{\text{RD}}}^H\widehat{\mathbf{H}}_{\text{RD}}$$

where the corresponding singular value matrices (29) and (30) are given as $\widetilde{\mathbf{\Lambda}}_{\text{SR}}[P_f]$ and $\widetilde{\mathbf{\Lambda}}_{\text{RD}}[E_f]$ with their diagonal elements arranged in descending order. The ith diagonal elements of $\widetilde{\mathbf{\Lambda}}_{\text{SR}}[P_f]$ and $\widetilde{\mathbf{\Lambda}}_{\text{RD}}[E_f]$ are correspondingly denoted as $\widetilde{\lambda}_{\text{SR},i}[P_f]$ for $i = 1, \ldots, K_{\text{SR}}$ and $\widetilde{\lambda}_{\text{RD},i}[E_f]$ for $i = 1, \ldots, K_{\text{RD}}$. Using the optimal structure of $\mathbf{F}_2$ and $\mathbf{G}$ given in (36) and the corresponding SVDs of $\widetilde{\mathbf{H}}_{\text{SR}}[P_f]$ and $\widetilde{\mathbf{H}}_{\text{RD}}[E_f]$ for the flexible power scheme, the optimization subproblem (45a) can be equivalently expressed as

$$\max_{\mathbf{x}} \frac{1-\alpha}{2}\sum_{i=1}^{K_{\text{SR}}}\log_2(1 + a_i x_i) \tag{49a}$$

$$\text{s.t.} \sum_{i=1}^{K_{\text{SR}}} x_i \le P_f, \quad x_i \ge 0, \qquad i = 1, \ldots, K_{\text{SR}} \tag{49b}$$

where $\mathbf{x} = [x_1, \ldots, x_{K_{\text{SR}}}]^T$, and for $i = 1, \ldots, K_{\text{SR}}$, $a_i = \widetilde{\lambda}_{\text{SR},i}[P_f]$ and $x_i = \lambda_{2,i}$, while the optimization subproblem (46a) is rewritten as

$$\max_{\mathbf{y}} \frac{1-\alpha}{2}\sum_{i=1}^{K_{\text{RD}}}\log_2(1 + b_i y_i) \tag{50a}$$

$$\text{s.t.} \sum_{i=1}^{K_{\text{RD}}} y_i \le E_f, \ \ y_i \ge 0, \quad i = 1, \ldots, K_{\text{RD}} \tag{50b}$$

where $\mathbf{y} = [y_1, \ldots, y_{K_{\text{RD}}}]^T$, and for $i = 1, \ldots, K_{\text{RD}}$, $b_i = \widetilde{\lambda}_{\text{RD},i}[E_f]$ and $y_i = \lambda_{g,i}$. It is obvious to note that the problems (49a) and (50a) are convex and can be easily solved by the water-filling algorithm.

To obtain the optimal k, we use the bisection method to solve the master problem (48). For $i = 1, \ldots, n$, where n is the number of iterations needed to obtain the optimal k, we denote $[L_i, R_i]$ as the search region in the ith iteration with $L_1 = 0$ and $R_1 = (1+\alpha)P_s/2$, and k for the ith iteration is $k_i = (L_i + R_i)/2$. The value of $\hat{\mathcal{I}}_{\text{SR}}(k_i)$ and $\hat{\mathcal{I}}_{\text{RD}}(k_i)$ is obtained by solving the problem (49a) and (50a), respectively. In the case of $\hat{\mathcal{I}}_{\text{SR}}(k_i) < \hat{\mathcal{I}}_{\text{RD}}(k_i)$, we set $L_{i+1} = k_i$, and if $\hat{\mathcal{I}}_{\text{SR}}(k_i) > \hat{\mathcal{I}}_{\text{RD}}(k_i)$, we set $R_{i+1} = k_i$. The steps of bisection are repeated until the difference between the value of $\hat{\mathcal{I}}_{\text{SR}}(k_n)$ and $\hat{\mathcal{I}}_{\text{RD}}(k_n)$ is less than ϑ, where ϑ is a positive constant close to 0. The process of solving the primal decomposition optimization problem by using the bisection method is summarized in Algorithm 2. The complexity orders of calculating the SVD of $\widetilde{\mathbf{H}}_{\text{SR}}$ and $\widetilde{\mathbf{H}}_{\text{RD}}$ are $\mathcal{O}(N_R^2 N_S + N_S^3)$ and $\mathcal{O}(N_D^2 N_R + N_R^3)$, respectively, and the complexity orders of solving the problem (49a) and (50a) are $\mathcal{O}(c_1 K_{\text{SR}})$ and $\mathcal{O}(c_2 K_{\text{RD}})$, respectively, where c_1 and c_2 are the numbers of iterations required to obtain the Lagrange multiplier in the water-filling solutions. Thus, the overall computational complexity order of Algorithm 2 is $\mathcal{O}(c_3(N_R^2 N_S + N_S^3 + N_D^2 N_R + N_R^3 + c_1 K_{\text{SR}} + c_2 K_{\text{RD}}))$, where c_3 is the number of bisection operations required to obtain the optimal k.

Next, as illustrated in Fig. 2, the objective function $\hat{\mathcal{I}}_{\text{SD}}$ with the flexible power constraint is monotonically decreasing with regard to α, while the feasible region of (44c) is monotonically increasing with α. Hence, the optimal α can be obtained by using the golden section search method, as presented in Algorithm 1.

V. Peak Power Constraint

In Section IV, it is worth to mention that in the problem (43a), the transmission power $\text{tr}\{\mathbf{F}_1\}$ may approach infinity when α approaches 0, and $\text{tr}\{\mathbf{F}_2\}$ and $\text{tr}\{\mathbf{G}\}$ may become infinite

Algorithm 2: Solving the Problem (44) by the Primal Decomposition Method.

Initialization: $n=1$, $L_1=0$, and $R_1=\frac{(1+\alpha)P_s}{2}$.
do
  Obtain $k_n=(L_n+R_n)/2$.
  Obtain SVD of $\widetilde{\mathbf{H}}_{\text{SR}}$ and $\widetilde{\mathbf{H}}_{\text{RD}}$ with k_n.
  Compute a_i, $i=1,\ldots,K_{\text{SR}}$ and b_j, $j=1,\ldots,K_{\text{RD}}$
  Solve (49a) and (50a).
  Compute $\hat{\mathcal{I}}_{\text{SR}}(k_n)$ as (49a) and $\hat{\mathcal{I}}_{\text{RD}}(k_n)$ as (50a).
  if $\hat{\mathcal{I}}_{\text{SR}}(k_n)-\hat{\mathcal{I}}_{\text{RD}}(k_n)<0$ **then**
    $L_{n+1}=k_n$.
  else if $\hat{\mathcal{I}}_{\text{SR}}(k_n)-\hat{\mathcal{I}}_{\text{RD}}(k_n)>0$ **then**
    $R_{n+1}=k_n$.
  end if
  $n\leftarrow n+1$.
while $|\hat{\mathcal{I}}_{\text{SR}}(k_{n-1})-\hat{\mathcal{I}}_{\text{RD}}(k_{n-1})|\geq\vartheta$
Find $\mathbf{x}^*$ and $\mathbf{y}^*$ with $k^*=k_{n-1}$ by solving (49a) and (50a).

when α is close to 1. However, infinite transmission power is not achievable in practice. Thus, we introduce $\widehat{P}_s$ and $\widehat{P}_r$ as peak power limits at the source and relay nodes, respectively, to impose practical peak transmission power constraints given as $\text{tr}\{\mathbf{F}_1\}\leq\widehat{P}_s$, $\text{tr}\{\mathbf{F}_2\}\leq\widehat{P}_s$, and $\text{tr}\{\mathbf{G}\}\leq\widehat{P}_r$ to the optimization problem (44a) with the optimal structure of $\mathbf{F}_1=\lambda_1\mathbf{v}_{q,1}\mathbf{v}_{q,1}^H$ and $0\leq\lambda_1\leq\widehat{P}_s$. Hence, the optimization problem with the consideration of peak power limits at the source and relay nodes is written as

$$\max_{\alpha,\lambda_1,\mathbf{F}_2,\mathbf{G}}\ \hat{\mathcal{I}}_{\text{SD}} \tag{51a}$$

$$\text{s.t. } \alpha\lambda_1+\frac{1-\alpha}{2}\text{tr}\{\mathbf{F}_2\}\leq\frac{1+\alpha}{2}P_s \tag{51b}$$

$$\frac{1-\alpha}{2}\text{tr}\{\mathbf{G}\}\leq\alpha E_{\text{clc}}(\lambda_1\chi) \tag{51c}$$

$$\text{tr}\{\mathbf{F}_2\}\leq\widehat{P}_s \tag{51d}$$

$$\text{tr}\{\mathbf{G}\}\leq\min\left(\widehat{E}_\alpha,\widehat{P}_r\right) \tag{51e}$$

$$\lambda_1\geq 0, 0\leq\alpha\leq 1 \tag{51f}$$

where $\widehat{E}_\alpha=2\eta\alpha E_{\text{clc}}(\chi\widehat{P}_s)/(1-\alpha)-N_RP_c$.

As the optimization problem (51) can be viewed as a problem extended from the problem (44) with the introduction of peak power constraints given as (51d) and (51e), we can exploit the solution of (44) with fixed α and denote it as $\mathbf{F}_2'$ and $\mathbf{G}'$ when solving the optimization problem (51) with fixed α. In the case where the peak power constraints (51d) and (51e) are satisfied with $\mathbf{F}_2'$ and $\mathbf{G}'$, then the optimal $\mathbf{F}_2$ and $\mathbf{G}$ for the optimization problem (51) are $\mathbf{F}_2'$ and $\mathbf{G}'$. In the case where the peak power constraint (51d) is violated with $\mathbf{F}_2'$, but $\mathbf{G}'$ satisfies (51e), the optimal $\mathbf{F}_2$ is obtained by solving the following optimization problem:

$$\max_{\mathbf{F}_2}\ \hat{\mathcal{I}}_{\text{SR}} \tag{52a}$$

$$\text{s.t. } \text{tr}\{\mathbf{F}_2\}\leq\widehat{P}_s,\ \ \mathbf{F}_2\geq 0. \tag{52b}$$

As the equality of (52b) holds with the optimal $\mathbf{F}_2$, we have $\widetilde{\mathbf{H}}_{\text{SR}}[\text{tr}\{\mathbf{F}_2\}]=\widetilde{\mathbf{H}}_{\text{SR}}[\widehat{P}_s]$, which can be rewritten as

$$\widetilde{\mathbf{H}}_{\text{SR}}[\widehat{P}_s]=\left(\sigma_r^2\mathbf{I}_{N_R}+\widehat{P}_s\varphi_{\text{SR}}\mathbf{\Lambda}_{\Sigma_{\text{SR}}}\right)^{-\frac{1}{2}}\mathbf{V}_{\Sigma_{\text{SR}}}^H\widehat{\mathbf{H}}_{\text{SR}}$$

and its singular value matrix (29) is given by $\widetilde{\mathbf{\Lambda}}_{\text{SR}}[\widehat{P}_s]$ with the diagonal elements arranged in descending order. The ith diagonal element of $\widetilde{\mathbf{\Lambda}}_{\text{SR}}[\widehat{P}_s]$ is denoted as $\widetilde{\lambda}_{\text{SR},i}[\widehat{P}_s]$ for $i=1,\ldots,K_{\text{SR}}$. By using the optimal structure of $\mathbf{F}_2$ proposed in (36) with the corresponding SVD of $\widetilde{\mathbf{\Lambda}}_{\text{SR}}[\widehat{P}_s]$, the problem (52a) can be rewritten as

$$\max_{\widehat{\mathbf{x}}}\ \frac{1-\alpha}{2}\sum_{i=1}^{K_{\text{SR}}}\log_2(1+\widehat{a}_i\widehat{x}_i) \tag{53a}$$

$$\text{s.t.}\sum_{i=1}^{K_{\text{SR}}}\widehat{x}_i\leq\widehat{P}_s,\quad \widehat{x}_i\geq 0,\qquad i=1,\ldots,K_{\text{SR}} \tag{53b}$$

where $\widehat{\mathbf{x}}=[\widehat{x}_1,\ldots,\widehat{x}_{K_{\text{SR}}}]^T$ and for $i=1,\ldots,K_{\text{SR}}$, $\widehat{a}_i=\widetilde{\lambda}_{\text{SR},i}[\widehat{P}_s]$ and $\widehat{x}_i=\lambda_{2,i}$. The problem (53a) can be easily solved by the water-filling algorithm.

In the case where the peak power constraint (51e) is violated with $\mathbf{G}'$, but $\mathbf{F}_2'$ satisfies (51d), the optimal $\mathbf{G}$ is obtained by solving the following optimization problem:

$$\max_{\mathbf{G}}\ \hat{\mathcal{I}}_{\text{RD}} \tag{54a}$$

$$\text{s.t. } \text{tr}\{\mathbf{G}\}\leq\tau,\ \ \mathbf{G}\geq 0 \tag{54b}$$

where $\tau=\min(\widehat{E}_\alpha,\widehat{P}_r)$. As the equality of (54b) holds with the optimal $\mathbf{G}$ for the problem (54a), there is $\widetilde{\mathbf{H}}_{\text{RD}}[\text{tr}\{\mathbf{G}\}]=\widetilde{\mathbf{H}}_{\text{RD}}[\tau]$, which can be written as

$$\widetilde{\mathbf{H}}_{\text{RD}}[\tau]=\left(\sigma_d^2\mathbf{I}_{N_D}+\tau\varphi_{\text{RD}}\mathbf{\Lambda}_{\Sigma_{\text{RD}}}\right)^{-\frac{1}{2}}\mathbf{V}_{\Sigma_{\text{RD}}}^H\widehat{\mathbf{H}}_{\text{RD}}$$

and its singular value matrix (30) is given by $\widetilde{\mathbf{\Lambda}}_{\text{RD}}[\tau]$ with the diagonal elements arranged in descending order. The ith diagonal element of $\widetilde{\mathbf{\Lambda}}_{\text{RD}}[\tau]$ is denoted as $\widetilde{\lambda}_{\text{RD},i}[\tau]$ for $i=1,\ldots,K_{\text{RD}}$. By using the optimal structure of $\mathbf{G}$ in (36) with the corresponding SVD of $\widetilde{\mathbf{\Lambda}}_{\text{RD}}[\tau]$, the problem (54a) can be rewritten as

$$\max_{\widehat{\mathbf{y}}}\ \frac{1-\alpha}{2}\sum_{i=1}^{K_{\text{RD}}}\log_2(1+\widehat{b}_i\widehat{y}_i) \tag{55a}$$

$$\text{s.t.}\sum_{i=1}^{K_{\text{RD}}}\widehat{y}_i\leq\tau,\quad \widehat{y}_i\geq 0,\qquad i=1,\ldots,K_{\text{RD}} \tag{55b}$$

where $\widehat{\mathbf{y}}=[\widehat{y}_1,\ldots,\widehat{y}_{K_{\text{RD}}}]^T$ and for $i=1,\ldots,K_{\text{RD}}$, $\widehat{b}_i=\widetilde{\lambda}_{\text{RD},i}[\tau]$ and $\widehat{y}_i=\lambda_{g,i}$. The problem (55a) is convex, which can be easily solved by the water-filling algorithm.

Finally, if both (51d) and (51e) are violated, we solve the problem (52a) to obtain the optimal $\mathbf{F}_2$ and the problem (54a) for the optimal $\mathbf{G}_2$. The process of solving the problem (51a) is summarized in Algorithm 3. It is important to note that with the optimal $\mathbf{F}_2$ and $\mathbf{G}$ obtained from Algorithm 3, the optimal $\hat{\mathcal{I}}_{\text{SD}}\{\alpha\}=\min(\hat{\mathcal{I}}_{\text{SR}},\hat{\mathcal{I}}_{\text{RD}})$ is a unimodal function of α, as illustrated in Fig. 2. Thus, the optimal α is obtained through the golden section search method following Algorithm 1.

Algorithm 3: Solving the Problem (51a) With Given α.

1: Solve (44) with Algorithm 2 to obtain $\mathbf{F}'_2$ and $\mathbf{G}'$.
2: **if** $\mathrm{tr}\{\mathbf{F}'_2\} \leq \widehat{P}_s$ **then**
3: $\quad \mathbf{F}_2^* = \mathbf{F}'_2$.
4: **else**
5: $\quad$ Find $\widehat{\mathbf{x}}^*$ by solving the problem (53a).
6: $\quad$ Compute $\boldsymbol{\lambda}_2^*$ with $\widehat{\mathbf{x}}^*$ then find $\mathbf{F}_2^*$ with (36).
7: **end if**
8: **if** $tr\{\mathbf{G}'\} \leq \tau$ **then**
9: $\quad \mathbf{G}^* = \mathbf{G}'$.
10: **else**
11: $\quad$ Find $\widehat{\mathbf{y}}^*$ by solving the problem (55a).
12: $\quad$ Compute $\boldsymbol{\lambda}_g^*$ with $\widehat{\mathbf{y}}^*$ then find $\mathbf{G}^*$ with (36).
13: **end if**

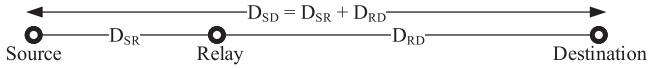

Fig. 3. Placement of the source, relay, and destination nodes in the relay communication system.

VI. Numerical Simulations

In this section, the performance of the proposed robust transceiver designs under the fixed power scheme [Fixed], the flexible power scheme without peak power limits [Flexible (w/o Peak)], and the flexible power scheme with peak power limits [Flexible (w Peak)] is investigated. The peak power limits are assumed as $\widehat{P}_s = \widehat{P}_r = rP_s$ ($r \geq 1$) in the numerical examples. We consider that the nodes in the relay communication system are placed, as illustrated in Fig. 3. The source–relay distance and the relay–destination distance are set as $D_{\mathrm{SR}} = 10\nu$ m and $D_{\mathrm{RD}} = 10(2-\nu)$ m, respectively with the total distance between the source and destination nodes given as $D_{\mathrm{SD}} = 20$ m. To determine the relay position with ease, the value of ν ($0 < \nu < 2$) is normalized over a distance of 10 m. When $0 < \nu < 1$, the relay is located closer to the source node as indicated by $D_{\mathrm{SR}} < D_{\mathrm{RD}}$, whereas $D_{\mathrm{SR}} > D_{\mathrm{RD}}$ when $1 < \nu < 2$ indicating that the relay is located closer to the destination node. We set $D_{\mathrm{SR}} \geq 2$ m and $D_{\mathrm{RD}} \geq 2$ m with $0.2 \leq \nu \leq 1.8$. Note that the three nodes do not need to be located on one line. Nevertheless, the collinear setup makes it convenient to study the impact of the location of the relay node to the achievable rate through one parameter ν.

With the consideration of channel pathloss, the channel matrices $\mathbf{H}_{\mathrm{SR}}$ and $\mathbf{H}_{\mathrm{RD}}$ are constructed as $\mathbf{H}_{\mathrm{SR}} = D_{\mathrm{SR}}^{-\xi/2}(\widehat{\mathbf{H}}_{\mathrm{SR}} + \boldsymbol{\Delta}_{\mathrm{SR}})$ and $\mathbf{H}_{\mathrm{RD}} = D_{\mathrm{RD}}^{-\xi/2}(\widehat{\mathbf{H}}_{\mathrm{RD}} + \boldsymbol{\Delta}_{\mathrm{RD}})$, where $D_{\mathrm{SR}}^{-\xi}$ and $D_{\mathrm{RD}}^{-\xi}$ denote the large-scale pathloss of the source–relay link and the relay–destination link, respectively, with ξ being the pathloss exponent. For the suburban communication scenario [30], we set $\xi = 3$. The estimated channel matrices $\widehat{\mathbf{H}}_{\mathrm{SR}}$ and $\widehat{\mathbf{H}}_{\mathrm{RD}}$ are modeled as [24]

$$\widehat{\mathbf{H}}_{\mathrm{SR}} \sim \mathcal{CN}\left(\mathbf{0}, \tfrac{1-\sigma_e^2}{\sigma_e^2}\boldsymbol{\Sigma}_{\mathrm{SR}} \otimes \boldsymbol{\Phi}_{\mathrm{SR}}^T\right)$$

$$\widehat{\mathbf{H}}_{\mathrm{RD}} \sim \mathcal{CN}\left(\mathbf{0}, \tfrac{1-\sigma_e^2}{\sigma_e^2}\boldsymbol{\Sigma}_{\mathrm{RD}} \otimes \boldsymbol{\Phi}_{\mathrm{RD}}^T\right)$$

where σ_e^2 represents the variance of estimation error. Note that $\widehat{\mathbf{H}}_{\mathrm{SR}}$, $\widehat{\mathbf{H}}_{\mathrm{RD}}$, $\boldsymbol{\Delta}_{\mathrm{SR}}$, and $\boldsymbol{\Delta}_{\mathrm{RD}}$ can be equivalently expressed as

$$\widehat{\mathbf{H}}_{\mathrm{SR}} = \sqrt{\tfrac{1-\sigma_e^2}{\sigma_e^2}}\boldsymbol{\Sigma}_{\mathrm{SR}}^{\frac{1}{2}}\widehat{\mathbf{H}}_{\omega_{\mathrm{SR}}}\boldsymbol{\Phi}_{\mathrm{SR}}^{\frac{1}{2}}$$

$$\widehat{\mathbf{H}}_{\mathrm{RD}} = \sqrt{\tfrac{1-\sigma_e^2}{\sigma_e^2}}\boldsymbol{\Sigma}_{\mathrm{RD}}^{\frac{1}{2}}\widehat{\mathbf{H}}_{\omega_{\mathrm{RD}}}\boldsymbol{\Phi}_{\mathrm{RD}}^{\frac{1}{2}}$$

$$\boldsymbol{\Delta}_{\mathrm{SR}} = \boldsymbol{\Sigma}_{\mathrm{SR}}^{\frac{1}{2}}\boldsymbol{\Delta}_{\omega_{\mathrm{SR}}}\boldsymbol{\Phi}_{\mathrm{SR}}^{\frac{1}{2}}, \quad \boldsymbol{\Delta}_{\mathrm{RD}} = \boldsymbol{\Sigma}_{\mathrm{RD}}^{\frac{1}{2}}\boldsymbol{\Delta}_{\omega_{\mathrm{RD}}}\boldsymbol{\Phi}_{\mathrm{RD}}^{\frac{1}{2}}$$

where $\widehat{\mathbf{H}}_{\omega_{\mathrm{SR}}}$ and $\widehat{\mathbf{H}}_{\omega_{\mathrm{RD}}}$ are complex Gaussian matrices whose entries are i.i.d. with zero mean and variance of $1/N_S$ and $1/N_R$, respectively. Here, $\boldsymbol{\Phi}_{\mathrm{SR}}$, $\boldsymbol{\Phi}_{\mathrm{RD}}$, $\boldsymbol{\Sigma}_{\mathrm{SR}}$, and $\boldsymbol{\Sigma}_{\mathrm{RD}}$ are simulated as

$$[\boldsymbol{\Phi}_{\mathrm{SR}}]_{ij} = \sigma_e^2\rho_t^{|i-j|}, \quad i,j = 1,\ldots,N_S$$

$$[\boldsymbol{\Phi}_{\mathrm{RD}}]_{ij} = \sigma_e^2\rho_t^{|i-j|}, \quad i,j = 1,\ldots,N_R$$

$$[\boldsymbol{\Sigma}_{\mathrm{SR}}]_{ij} = \rho_r^{|i-j|}, \quad i,j = 1,\ldots,N_R$$

$$[\boldsymbol{\Sigma}_{\mathrm{RD}}]_{ij} = \rho_r^{|i-j|}, \quad i,j = 1,\ldots,N_D$$

where $\rho_t \in [0,1]$ and $\rho_r \in [0,1]$ represent the correlation coefficients of the channel correlation matrices. In the numerical examples, we set $\rho_t = 0.1$ and $\rho_r = 0.01$. The noise variances at the relay and destination nodes are set as $\sigma_r^2 = \sigma_d^2 = -50$ dBm. The per-antenna static power consumption is set as $P_c = 1\mu$W. The conversion efficiency is set as $\eta = 0.8$. The number of antennas at the source, relay, and destination nodes is considered as $N_S = N_R = N_D = 2$. These predefined values remain the same for all numerical examples unless specifically mentioned. Besides the numerical example 6, the considered EH circuit is assumed to be ideal ($P_{\mathrm{th}} = 0, E_m = \infty$) for all others numerical examples. We obtain the results by averaging through 1000 independent channel realizations for the numerical simulations. The proposed transceiver design with robustness is compared to the transceiver design in [10] using the estimated CSI, which is denoted as [Non-Rob Flexible], and the transceiver design with the full CSI (FCSI), which is denoted as [FCSI], in the numerical examples.

For numerical example 1, we investigate the MI performance versus P_s for the proposed transceiver designs with robustness and the nonrobust transceiver design given in [10] using only the estimated CSI. The transceiver design in [10] using the FCSI is set as the benchmark in the simulation. We would like to mention that the transceiver design with FCSI is unavailable in practice due to the inevitable CSI mismatch. In this numerical simulation, we set $\nu = 1$ and $\sigma_e^2 = 0.15$. Fig. 4 displays the system MI versus P_s for the tested systems. For the systems with and without peak power limits ($r = 2$), it is noticed that the FCSI transceiver design provides an upper bound of the system MI, and the CSI mismatch heavily degrades the MI performance of the system when P_s is high. In particular, the upward trend of the FCSI curves is different from that of the other curves, due to the fact that the system MI for the ideal situation with FCSI does not have an "error floor." On the other hand, the curves associated with the MI for systems in the nonideal situation (both robust and nonrobust algorithms) demonstrate "error floor," due to the CSI mismatch. It is noticeable that the MI performance of the system with the robust transceiver design is higher than the system using the nonrobust transceiver design. In other words,

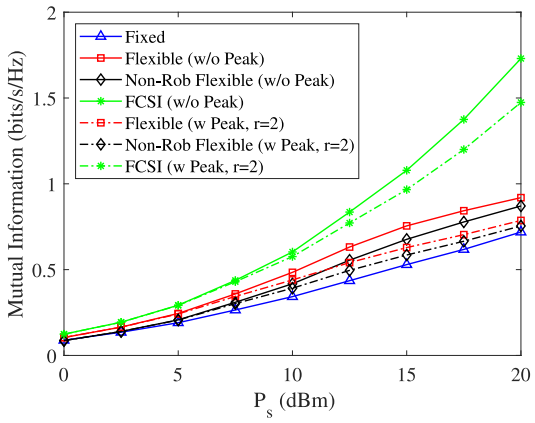

Fig. 4. Example 1: MI versus P_s with $\nu = 1$ and $\sigma_e^2 = 0.15$.

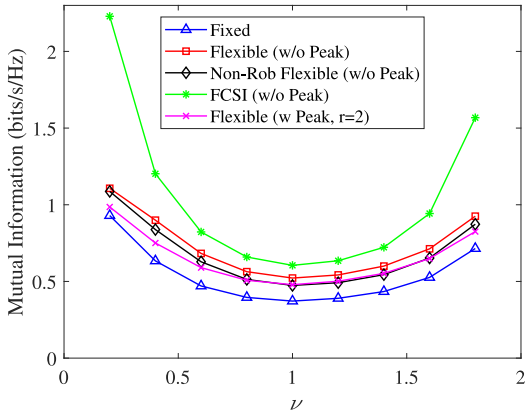

Fig. 6. Example 2: MI versus ν at $P_s = 10$ dBm and $\sigma_e^2 = 0.1$.

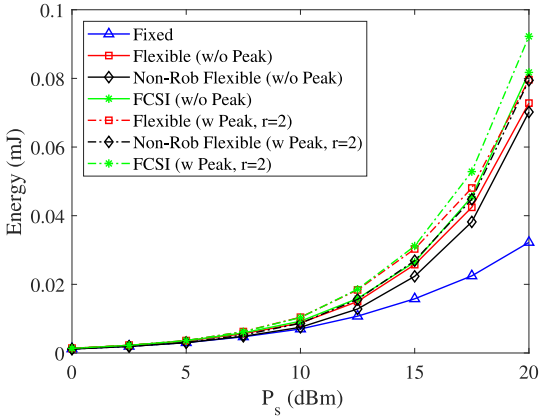

Fig. 5. Example 1: Harvested energy at the relay node versus P_s with $\nu = 1$ and $\sigma_e^2 = 0.15$.

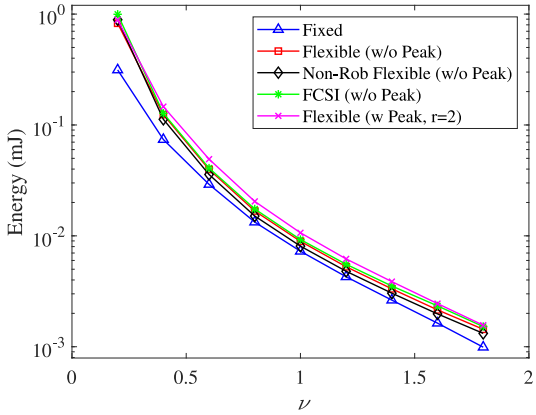

Fig. 7. Example 2: Harvested energy at the relay node versus ν at $P_s = 10$ dBm and $\sigma_e^2 = 0.1$.

the robust transceiver design has a better performance compared with the nonrobust transceiver design.

We can also observe from Fig. 4 that the system with the fixed power scheme has the lowest MI performance. This is because the feasible region of the system with the fixed power constraint is smaller than the system with the flexible power constraint. In fact, the fixed power constraint (31b) is a special case of the flexible power constraint (43b). In the system with the flexible power constraint (43b), the source precoding matrices $\mathbf{F}_1$ and $\mathbf{F}_2$ are linked by one energy constraint, which enables the source node to work at different power levels accommodated to the purpose of energy transferring at the first time frame and information transmission at the second time frame.

Fig. 5 shows the amount of energy harvested at the relay node versus P_s for the tested systems. We can see that the energy harvested at the relay node is also influenced by the CSI mismatch. The proposed transceiver design with robustness harvests more energy at the relay node compared with the existing transceiver design without robustness. It can also be observed in Fig. 5 that the energy harvested with the fixed power constraint is smaller than the system with the flexible power constraint. In the following numerical examples, the nonrobust transceiver design and the FCSI transceiver design will be carried out without the consideration of the peak power limits. For a fair comparison, the proposed robust transceiver design under the flexible power scheme will be used.

For numerical example 2, the MI performance of the transceiver designs is investigated at various relay positions. Fig. 6 displays the MI performance of the simulated transceiver designs. Fig. 7 displays the harvested energy at the relay node for the tested system across various ν with $P_s = 10$ dBm and $\sigma_e^2 = 0.1$. It is observed that the MI performance is higher when the relay node is located closer to the source node or the destination node. This can be explained as follows. When the relay node is located closer to the source node ($0 < \nu < 1$), more RF energy can be harvested at the relay node, which can be observed in Fig. 7, as the RF energy transmission loss at the source–relay link is reduced. This enhances the MI performance of the system. Even though the RF energy harvested at the relay node is smaller when the relay node is located closer to the destination node ($1 < \nu < 2$), the relay–destination distance is shorter, which helps in improving the MI performance of the system. It is also observed that the energy harvested at the relay node by the proposed transceiver design and the existing nonrobust transceiver design across various ν are similar, the proposed transceiver design with robustness performs better than the nonrobust transceiver design at any relay node position. This indicates that the CSI mismatch causes greater degradation to

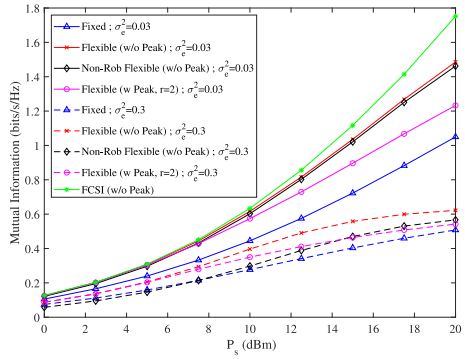

Fig. 8. Example 3: MI versus P_s with $\nu = 1$.

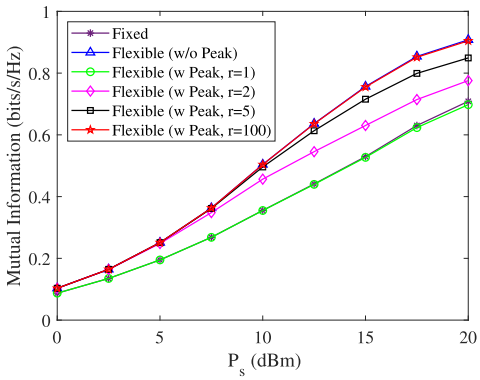

Fig. 9. Example 4: MI versus P_s with $\sigma_e^2 = 0.15$ and $\nu = 1$.

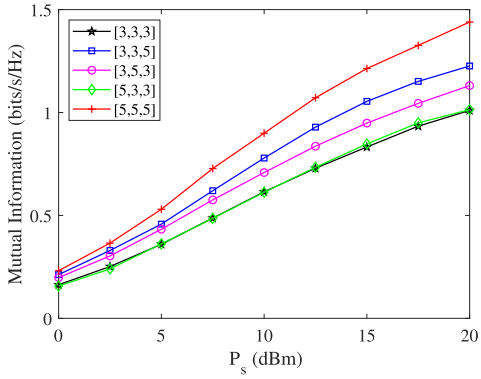

Fig. 10. Example 5: MI versus P_s for robust transceiver design with a peak power constraint at various $[N_S, N_R, N_D]$, $r = 2$, $\nu = 1$, and $\sigma_e^2 = 0.15$.

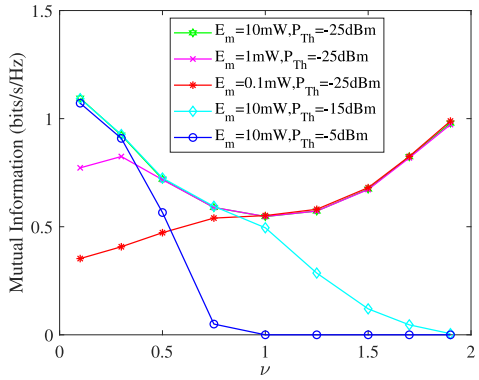

Fig. 11. Example 6: MI versus ν for robust transceiver design with a fixed power scheme at different P_{Th} and E_m with $P_s = 15$ dBm and $\sigma_e^2 = 0.1$.

the system MI compared with the harvested energy at the relay node.

For numerical example 3, we investigate the impact of σ_e^2 on the MI performance of the tested systems. The MI performance versus P_s for the tested systems is displayed in Fig. 8 with $\nu = 1$ and $r = 2$ at $\sigma_e^2 = 0.03$ and $\sigma_e^2 = 0.3$. It is observed that when σ_e^2 is smaller, the MI performance of the tested systems is approaching the system MI with FCSI. This observation indicates that the CSI mismatch with larger channel estimation error causes significant loss in the MI performance of the system. Moreover, the gap between the MI performance of the robust transceiver design and the nonrobust transceiver design is larger with higher σ_e^2. This is because when the CSI mismatch is greater with higher σ_e^2, it causes more degradation to the system using the nonrobust transceiver design.

For numerical example 4, we investigate the impact of peak power limits on the system MI. Fig. 9 displays the MI performance versus P_s with various peak power limits at $r = 1$, $r = 2$, $r = 5$, and $r = 100$ for the robust transceiver design at $\nu = 1$ and $\sigma_e^2 = 0.15$. It can be noticed that the MI performance increases with the increase of r. It is noticed that when r is sufficiently large, the MI performance of the system with peak power constraint is similar to that of the system without peak power constraint. This is because the peak power constraint is more easy to be satisfied when the power limit is large. It is also noticed that when $r = 1$, the system MI for a flexible power constraint with peak power limits is approximately identical to the system MI for a fixed power constraint at low P_s. At high P_s, the proposed robust transceiver design with the fixed power constraint is slightly greater than the proposed robust transceiver design with the flexible power constraint with peak power limits.

For numerical example 5, we investigate the influence of the number of antennas at the system nodes towards the system MI. Fig. 10 displays the MI performance versus P_s at various combinations of $[N_S, N_R, N_D]$ for the robust transceiver design under the flexible power scheme with the peak power constraint with $r = 2$, $\nu = 1$, and $\sigma_e^2 = 0.15$. It can be noticed that when the number of antennas at all system nodes increases from 3 to 5, the system MI has a significant increase. It is noticed that when we only increase the number of antennas at the source node, i.e., from the [3, 3, 3] distribution to the [5, 3, 3] distribution, the system MI is almost identical. This indicates that the increment of the number of antennas at the source node does not heavily influence the system MI. However, when we increase the number of antennas at the relay and/or destination nodes, the system MI for the [3, 5, 3] and [3, 3, 5] distributions is higher than the system MI for the [5, 3, 3,] distribution. This is because the system MI is limited by the MI of the relay–destination link, which is because the transmission energy available at the relay node is smaller than the transmission power available at the source node. Thus, increasing the number of antennas at the relay and/or destination nodes improves the system MI.

For numerical example 6, we examine the impact of P_{Th} and E_m introduced by the practical EH circuit toward the system MI. Fig. 11 displays the MI performance versus ν at various P_{Th} and E_m for the robust transceiver design under the fixed power

scheme with $P_s = 15$ dBm and $\sigma_e^2 = 0.1$. It can be observed from Fig. 11 that when $E_m = 10$ mW and $P_{\text{Th}} = -25$ dBm, the system MI for the system with the practical EH circuit follows the same trend as the system MI for the ideal EH circuit. However, when the maximum output power of the practical EH circuit is reduced to 1 mW, it is noted that placing the relay node closer to the source node does not increase the system MI. This is because the practical EH circuit achieves the maximum output power. It is easily noticed that the system MI increases when the relay node is located nearer to the destination node when $E_m = 0.1$ mW.

Furthermore, it is noted that when P_{Th} is increased, the system MI is decreased as the relay node is located further from the source node. This is because the energy received at the relay node is not sufficient to trigger the practical EH circuit to harvest the energy. Hence, without any available transmission energy at the relay node, it can be noticed that the system MI is reduced to 0 when $P_{\text{Th}} = -5$ dBm.

VII. Conclusion

In this article, we have investigated the robust transceiver design for a dual-hop DF MIMO relay communication system with the TS-based EH protocol. The transceiver design with robustness assists in reducing the degradation caused by the CSI mismatch between the exact and estimated CSI available in the system. With the consideration of CSI mismatch, the optimization problem is more difficult to solve. KKT conditions are applied to solve the source and relay precoding matrix optimization problem under the fixed power scheme, and the primal decomposition method is applied to solve the source and relay precoding matrix optimization problem under the flexible power constraint, while the golden section search method is adopted to obtain the optimized TS factor. The proposed transceiver design with robustness provides better performance compared with the nonrobust transceiver design, as shown through numerical examples.

References

[1] R. Zhang and C. K. Ho, "MIMO broadcasting for simultaneous wireless information and power transfer," *IEEE Trans. Wireless Commun.*, vol. 12, no. 5, pp. 1989–2001, May 2013.

[2] Y. Rong, "MIMO relay," in *Encyclopedia of Wireless Networks*, X. Shen, X. Lin, and K. Zhang, Eds. Cham, Switzerland: Springer, 2018.

[3] A. A. Nasir, X. Zhou, S. Durrani, and R. A. Kennedy, "Relaying protocols for wireless energy harvesting and information processing," *IEEE Trans. Wireless Commun.*, vol. 12, no. 7, pp. 3622–3636, Jul. 2013.

[4] P. Arapoglou, P. Burzigotti, M. Bertinelli, A. B. Alamanac, and R. De Gaudenzi, "To MIMO or not to MIMO in mobile satellite broadcasting systems," *IEEE Trans. Wireless Commun.*, vol. 10, no. 9, pp. 2807–2811, Sep. 2011.

[5] K. Xiong, P. Fan, C. Zhang, and K. B. Letaief, "Wireless information and energy transfer for two-hop non-regenerative MIMO-OFDM relay networks," *IEEE J. Sel. Areas Commun.*, vol. 33, no. 8, pp. 1595–1611, Aug. 2015.

[6] G. Amarasuriya, E. G. Larsson, and H. V. Poor, "Wireless information and power transfer in multiway massive MIMO relay networks," *IEEE Trans. Wireless Commun.*, vol. 15, no. 6, pp. 3837–3855, Jun. 2016.

[7] B. Li and Y. Rong, "Joint transceiver optimization for wireless information and energy transfer in nonregenerative MIMO relay systems," *IEEE Trans. Veh. Technol.*, vol. 67, no. 9, pp. 8348–8362, Sep. 2018.

[8] B. Li, M. Zhang, H. Cao, Y. Rong, and Z. Han, "Transceiver design for AF MIMO relay systems with a power splitting based energy harvesting relay node," *IEEE Trans. Veh. Technol.*, vol. 69, no. 3, pp. 2376–2388, Mar. 2020.

[9] Y. Liu, "Joint resource allocation in SWIPT-based multiantenna decode-and-forward relay networks," *IEEE Trans. Veh. Technol.*, vol. 66, no. 10, pp. 9192–9200, Oct. 2017.

[10] B. Li, H. Cao, Y. Rong, T. Su, G. Yang, and Z. He, "Transceiver optimization for DF MIMO relay systems with a wireless powered relay node," *IEEE Access*, vol. 7, pp. 56904–56919, 2019.

[11] J. L. Bing, Y. Rong, L. Gopal, and C. W. R. Chiong, "Transceiver design for SWIPT MIMO relay systems with hybridized power-time splitting-based relaying protocol," *IEEE Access*, vol. 8, pp. 190922–190933, 2020.

[12] Y. Rong, "Robust design for linear non-regenerative MIMO relays with imperfect channel state information," *IEEE Trans. Signal Process.*, vol. 59, no. 5, pp. 2455–2460, May 2011.

[13] L. Gopal, Y. Rong, and Z. Zang, "Robust MMSE transceiver design for nonregenerative multicasting MIMO relay systems," *IEEE Trans. Veh. Technol.*, vol. 66, no. 10, pp. 8979–8989, Oct. 2017.

[14] F. Benkhelifa and M. Alouini, "Precoding design of MIMO amplify-and-forward communication system with an energy harvesting relay and possibly imperfect CSI," *IEEE Access*, vol. 5, pp. 578–594, 2017.

[15] F. Benkhelifa, A. S. Salem, and M. Alouini, "Rate maximization in MIMO decode-and-forward communications with an EH relay and possibly imperfect CSI," *IEEE Trans. Commun.*, vol. 64, no. 11, pp. 4534–4549, Nov. 2016.

[16] R. Jiang, K. Xiong, P. Fan, L. Zhou, and Z. Zhong, "Outage probability and throughput of multirelay SWIPT-WPCN networks with nonlinear EH model and imperfect CSI," *IEEE Syst. J.*, vol. 14, no. 1, pp. 1206–1217, Mar. 2020.

[17] P. Shaik, P. K. Singya, N. Kumar, K. K. Garg, and V. Bhatia, "On impact of imperfect CSI over SWIPT device-to-device (D2D) MIMO relay systems," in *Proc. Int. Conf. Signal Process. Commun.*, Bangalore, India, 2020, pp. 1–5.

[18] Q. Li and L. Yang, "Robust optimization for energy efficiency in MIMO two-way relay networks with SWIPT," *IEEE Syst. J.*, vol. 14, no. 1, pp. 196–207, Mar. 2020.

[19] L. Musavian, M. R. Nakhai, M. Dohler, and A. H. Aghvami, "Effect of channel uncertainty on the mutual information of MIMO fading channels," *IEEE Trans. Veh. Technol.*, vol. 56, no. 5, pp. 2798–2806, Sep. 2007.

[20] C. Xing, S. Ma, and Y. Wu, "Robust joint design of linear relay precoder and destination equalizer for dual-hop amplify-and-forward MIMO relay systems," *IEEE Trans. Signal Process.*, vol. 58, no. 4, pp. 2273–2283, Apr. 2010.

[21] P. N. Alevizos and A. Bletsas, "Sensitive and nonlinear far-field RF energy harvesting in wireless communications," *IEEE Trans. Wireless Commun.*, vol. 17, no. 6, pp. 3670–3685, Jun. 2018.

[22] S. Wang, Z. He, and Y. Rong, "Joint transceiver optimization for DF multicasting MIMO relay systems with wireless information and power transfer," *IEEE Trans. Commun.*, vol. 69, no. 7, pp. 4953–4967, Jul. 2021.

[23] S. Simoens, O. Muñoz-Medina, J. Vidal, and A. del Coso, "On the Gaussian MIMO relay channel with full channel state information," *IEEE Trans. Signal Process.*, vol. 57, no. 9, pp. 3588–3599, Sep. 2009.

[24] M. Ding and S. D. Blostein, "Maximum mutual information design for MIMO systems with imperfect channel knowledge," *IEEE Trans. Inf. Theory*, vol. 56, no. 10, pp. 4793–4801, Oct. 2010.

[25] T. Yoo and A. Goldsmith, "Capacity and power allocation for fading MIMO channels with channel estimation error," *IEEE Trans. Inf. Theory*, vol. 52, no. 5, pp. 2203–2214, May 2006.

[26] T. Yoo, E. Yoon, and A. Goldsmith, "MIMO capacity with channel uncertainty: Does feedback help?," in *Proc. IEEE Global Telecommun. Conf.*, Dallas, TX, USA, Dec. 2004, pp. 96–100.

[27] K. Xiong, P. Fan, Y. Lu, and K. B. Letaief, "Energy efficiency with proportional rate fairness in multirelay OFDM networks," *IEEE J. Sel. Areas Commun.*, vol. 34, no. 5, pp. 1431–1447, May 2016.

[28] A. Antoniou and W.-S. Lu, *Practical Optimization Algorithms and Engineering Applications*, 1st ed. New York, NY, USA: Springer, 2007.

[29] D. P. Palomar and M. Chiang, "A tutorial on decomposition methods for network utility maximization," *IEEE J. Sel. Areas Commun.*, vol. 24, no. 8, pp. 1439–1451, Aug. 2006.

[30] C. Song, J. Park, B. Clerckx, I. Lee, and K. Lee, "Generalized precoder designs based on weighted MMSE criterion for energy harvesting constrained MIMO and multi-user MIMO channels," *IEEE Trans. Wireless Commun.*, vol. 15, no. 12, pp. 7941–7954, Dec. 2016.